Homeostatic Synaptic Plasticity of Miniature Excitatory Postsynaptic Currents in Mouse Cortical Cultures Requires Neuronal Rab3A

Andrew G. Koesters[1*], Mark M. Rich[2], and Kathrin L. Engisch[3]

[1]Department of Pharmacology and Systems Physiology, University of Cincinnati College of Medicine, Cincinnati, OH 45267, USA
[2]Department of Neuroscience, Cell Biology and Physiology, Boonshoft School of Medicine, Wright State University, Dayton, OH 45345
[3]Department of Neuroscience, Cell Biology and Physiology, Boonshoft School of Medicine and the College of Science and Mathematics, Wright State University, Dayton, OH 45435

*Andrew G. Koesters –Corresponding author
Department of Pharmacology and Systems Physiology, University of Cincinnati College of Medicine, Cincinnati, OH 45267, USA
koesteag@ucmail.uc.edu, ph 513-558-2819

Author contributions: A.G.K., K.L.E. and M.M.R. designed research; A.G.K. performed research; A.G.K. and K.L.E. analyzed data; A.G.K, K.L.E., and M.M.R. wrote the paper.

ORCID iDs: ; A.G.K, https://orcid.org/0000-0003-3281-188X; M.M.R., https://orcid.org/0000-0002-6956-5531; K.L.E., https://orcid.org/0000-0002-1058-5343

The authors have no competing interests.

Keywords: Homeostatic Synaptic Plasticity; Synaptic Scaling; mEPSCs; Rab3A; AMPA receptors

Acknowledgements: The authors thank E. Whitlock and H. Ghouse for their contributions to confocal image analyses. This work was partially supported by NINDS P01 NS057228, Tim Cope, PI, KE, PI project 4.

30 Abstract

31 Following prolonged activity blockade, amplitudes of miniature excitatory postsynaptic currents
32 (mEPSCs) increase, a form of plasticity termed "homeostatic synaptic plasticity." We previously
33 showed that a presynaptic protein, the small GTPase Rab3A, is required for full expression of
34 the increase in miniature endplate current amplitudes following prolonged blockade of action
35 potential activity at the mouse neuromuscular junction in vivo (Wang et al., 2011), but it is
36 unknown whether this form of Rab3A-dependent homeostatic plasticity shares any
37 characteristics with central synapses. We show here that homeostatic synaptic plasticity of
38 mEPSCs is impaired in mouse cortical neuron cultures prepared from Rab3A$^{-/-}$ and mutant mice
39 expressing a single point mutation of Rab3A, Rab3A Earlybird mice. To determine if Rab3A is
40 involved in the well-established homeostatic increase in postsynaptic AMPA-type receptors
41 (AMPARs), we performed a series of experiments in which electrophysiological recordings of
42 mEPSCs and confocal imaging of synaptic AMPAR immunofluorescence were assessed within
43 the same cultures. We found that Rab3A was required for the increase in synaptic AMPARs
44 following prolonged activity blockade, but the increase in mEPSC amplitudes was not always
45 accompanied by an increase in postsynaptic AMPAR levels, suggesting other factors may
46 contribute. Finally, we demonstrate that Rab3A is acting in neurons because only selective loss
47 of Rab3A in neurons, not glia, disrupted the homeostatic increase in mEPSC amplitudes. This is
48 the first demonstration that neuronal Rab3A is required for homeostatic synaptic plasticity and
49 that it does so partially through regulation of the surface expression of AMPA receptors.

50

51 Introduction

52 One of the most studied phenomena triggered by prolonged activity blockade is the
53 increase in amplitudes of miniature excitatory postsynaptic currents (mEPSCs) in neurons. First
54 demonstrated in cultures of dissociated cortical neurons (Turrigiano et al., 1998) and spinal
55 cord neurons (O'Brien et al., 1998), the compensatory response to prolonged loss of activity has
56 been dubbed “homeostatic synaptic plasticity” (Turrigiano and Nelson, 2004; Pozo and Goda,
57 2010). These first two studies provided evidence that glutamate receptors were also increased
58 after inactivity, via an increased response to exogenously applied glutamate (Turrigiano et al.,
59 1998) and increased immunofluorescent labeling of GluA1 receptors at synaptic sites (O'Brien
60 et al., 1998). The accompanying increase in synaptic AMPA receptors has been confirmed with
61 immunofluorescence in multiple studies of hippocampal and cortical cultures treated with TTX
62 (Wierenga et al., 2005; Hou et al., 2008; Ibata et al., 2008; Jakawich et al., 2010a; Tatavarty et
63 al., 2013; Xu and Pozzo-Miller, 2017; Dubes et al., 2022). It is now well accepted that the
64 homeostatic increase in mEPSC amplitudes in neurons is due to an increase in postsynaptic
65 AMPA receptors.

66 In our previous work, we found that a TTX cuff applied for 48 hr around the sciatic nerve
67 in mice led to an increase in the amplitude of the miniature endplate currents (mEPCs)
68 recorded in tibialis anterior muscles. Surprisingly, and unlike central synapses, we could find no
69 evidence that the acetylcholine receptors levels at the neuromuscular junction (NMJ) were
70 increased in the TTX-cuff treated mice (Wang et al., 2005). This result led us to search for
71 presynaptic molecules that might homeostatically regulate the presynaptic quantum. In
72 previous studies in chromaffin cells, we identified the small GTPase Rab3A, a presynaptic vesicle

73 protein, as a regulator of synaptic vesicle fusion pore opening (Wang et al., 2008), so we
74 examined whether deletion of Rab3A (Rab3A$^{-/-}$) might prevent homeostatic upregulation of
75 mEPC amplitude at the NMJ. The results were clear: the homeostatic increase in mEPC
76 amplitude induced by the TTX cuff was strongly reduced in the Rab3A$^{-/-}$ mouse, and was
77 completely abolished in the Earlybird mutant (Rab3A$^{Ebd/Ebd}$), which has a single point mutation
78 in Rab3A that causes a shift towards early awakening that is more dramatic than that of the
79 Rab3A deletion mouse (Kapfhamer et al., 2002; Wang et al., 2011). These results led us to
80 conclude that the homeostatic increase in mEPC amplitude at the NMJ is a presynaptic
81 phenomenon.

82 It has remained somewhat of a mystery what the role of Rab3A is in synaptic
83 transmission. The Rab3A$^{-/-}$ mouse has minimal phenotypic abnormalities, with evoked synaptic
84 transmission and mEPSCs essentially normal in hippocampal slices (Geppert et al., 1994). At the
85 Rab3A$^{-/-}$ NMJ, reductions in evoked transmission were detected, but only under conditions of
86 reduced extracellular calcium (Coleman et al., 2007). There are some modest changes in short
87 term plasticity during repetitive stimulus trains, with increased depression observed in
88 response to moderate frequencies in hippocampal slices (Geppert et al., 1994) and at the
89 mammalian NMJ (Coleman and Bykhovskaia, 2009), but increased facilitation in response to
90 high frequency stimulation at the mammalian NMJ (Coleman and Bykhovskaia, 2010). The most
91 dramatic effect of loss of Rab3A is the abolishment of a presynaptic form of long-term
92 potentiation (LTP) at the mossy fiber-CA3 synapse that is induced by 25 Hz stimulation in the
93 presence of NMDA blockers (Weisskopf et al., 1994; Castillo et al., 1997). Our result that
94 prolonged inactivity-induced plasticity of mEPC amplitude at the mammalian NMJ is disrupted

95 with loss of function of Rab3A further cements a role for Rab3A in activity-dependent plasticity
96 of synaptic strength. However, a crucial question that remains is whether the TTX-cuff induced
97 effect on the amplitude of the spontaneous synaptic current at the NMJ shares underlying
98 mechanisms with central synapses. We set out to answer this question for the more well-
99 studied phenomenon of homeostatic plasticity of mEPSCs in dissociated mouse cortical neurons
100 prepared from wild type, Rab3A$^{-/-}$ mice and Rab3a$^{Ebd/Ebd}$ mice treated with TTX for 48 hr. We
101 show here that homeostatic synaptic plasticity of mEPSC amplitude was strongly reduced in
102 cultures from Rab3A$^{-/-}$ mice, and completely abolished in cultures from Rab3A$^{Ebd/Ebd}$ mice,
103 supporting a shared mechanism with the neuromuscular junction. Unexpectedly, the modest
104 increase in GluA2 immunofluorescence we observed in wild type cultures was not present in
105 Rab3A$^{-/-}$ cultures. Loss of Rab3A in neurons, but not in glia, disrupted the increase in mEPSC
106 amplitudes after TTX treatment. These results support the idea that the increase in mEPSC
107 amplitude is due to more postsynaptic receptors, and that neuronal Rab3A is necessary for this
108 regulation. However, we found that GluA2 receptors and mEPSC amplitudes did not always
109 change in parallel. This mismatch suggests there may be contributors other than postsynaptic
110 receptor numbers to the homeostatic plasticity of mEPSC amplitude.

111

112 Results

113 We previously reported that mixed cultures of cortical neurons and glia prepared from
114 postnatal day 0-2 mouse pups responded to a block of action potential-mediated activity by a
115 48 hr TTX treatment with an increase in mEPSC amplitude (Hanes et al., 2020). Here, we asked

116 the question whether cortical cultures prepared from mice lacking the small GTPase Rab3A, or,
117 expressing a point mutation of Rab3A, Rab3A Earlybird, have an altered homeostatic plasticity
118 response to a loss of network activity. The Rab3A Earlybird mutation was discovered in a
119 mutagenesis screen in mice for genes involved in the rest-activity cycle (Kapfhamer et al.,
120 2002). The Earlybird mutant was named for its phenotype, a significantly shorter circadian
121 period which resulted in early awakening. In that study, the authors concluded that the
122 Earlybird mutation was likely dominant-negative, as the shift in circadian period was
123 substantially more dramatic than that observed in the Rab3A$^{-/-}$ mice. As described in the
124 Introduction, the effects of loss of Rab3A have been modest, so we included experiments using
125 the Rab3A Earlybird mutant mice to see if there would be a more robust phenotype, and in
126 doing so, strengthen conclusions based on the Rab3A deletion mice. To obtain Rab3A$^{-/-}$ and
127 Rab3A$^{Ebd/Ebd}$ homozygotes, we established two mouse colonies of heterozygous breeders with
128 cultures prepared from pups derived from a final breeding pair of homozygotes. Although we
129 backcrossed Rab3A$^{+/-}$ with Rab3A$^{+/Ebd}$ for 11 generations, clear differences in mEPSC amplitudes
130 in untreated cultures (see below) and in calcium current amplitudes in adrenal chromaffin cells
131 (unpublished obs.) remained. Therefore, throughout this study we keep the two strains
132 separate and there are two Rab3A$^{+/+}$ or 'wild type' phenotypes.

133 We found that loss of Rab3A resulted in a greatly impaired homeostatic increase after
134 activity blockade. Example current traces of spontaneously occurring mEPSCs recorded from
135 pyramidal neurons in untreated (CON) 13-14 DIV cortical cultures and sister cultures treated
136 with 500 nM TTX for 48 hr prepared from wild type and Rab3A$^{-/-}$ mice in the Rab3A$^{+/-}$ colony are
137 shown in Figures 1A and B, respectively. Average mEPSC waveforms from the same recordings

138 are shown in Figures 1C and D. The mean mEPSC amplitudes for 30 control and 23 TTX-treated
139 neurons from Rab3A$^{+/+}$ cultures are displayed in the box and whisker plot in Figure 1E; after
140 activity blockade the average mEPSC amplitude increased from 13.9 ± 0.7 pA to 18.2 ± 0.9 pA.
141 In contrast, in cultures prepared from Rab3A$^{-/-}$ mice, the average mEPSC amplitude was not
142 significantly increased, for 25 untreated cells and 26 TTX-treated cells (Figure 1F, 13.6 ± 0.1 pA
143 vs. 14.3 ± 0.6 pA). We found that TTX treatment also resulted in an increase in mEPSC
144 frequency in cultures prepared from Rab3A$^{+/+}$ mice, as shown in Figure 1G (CON, 2.26 ± 0.37
145 sec^{-1}; TTX, 4.62 ± 0.74 sec^{-1}). This TTX-induced frequency increase was strongly reduced in
146 cultures from Rab3A$^{-/-}$ mice, but there were a few outliers with very high frequencies still
147 present after TTX treatment (Figure 1H, CON, 2.74 ± 0.49 Hz; TTX, 3.23 ± 0.93 Hz).
148 We next examined homeostatic plasticity in cultures prepared from wild type mice in
149 the Rab3A$^{+/Ebd}$ colony. Example current traces of mEPSCs, and average mEPSC waveforms, are
150 shown in Figures 2A and C, respectively, for cortical cultures prepared from wild type mice in
151 the Rab3A$^{+/Ebd}$ colony. Treatment with TTX for 48 hr led to a significant increase in the average
152 mEPSC amplitude of 23 TTX-treated cells when compared to 20 untreated cells (Figure 2E, CON,
153 11.0 ± 0.6 pA; TTX, 15.0 ± 1.3 pA). We note here that while the two wild type strains respond
154 very similarly to activity blockade, the mean mEPSC amplitude in untreated cultures was
155 significantly different in the two wild type strains, 13.9 ± 0.7 pA, wild type from Rab3A$^{+/-}$ colony;
156 11.0 ± 0.6 pA, wild type from Rab3A$^{+/Ebd}$ colony ($p = 0.004$, Kruskal-Wallis test).
157 We found a complete disruption of homeostatic plasticity in cortical cultures prepared
158 from Rab3A$^{Ebd/Ebd}$ mice, as can been seen in viewing example mEPSC traces and average mEPSC
159 waveforms (Figures 2B and D, respectively). The lack of TTX effect was confirmed in a

160 comparison of mEPSC amplitude means for 21 untreated and 22 TTX-treated cells (Figure 2F,
161 CON, 15.1 ± 1.0 pA vs. TTX, 14.6 ± 1.1 pA). There was a trend towards increased mEPSC
162 frequency in TTX-treated cultures from this wild type strain, but the difference was not as
163 robust as for the wild type cultures from Rab3A$^{+/-}$ colony, and did not reach statistical
164 significance (Figure 2G, CON, 1.15 ± 0.19 sec^{-1}; TTX, 2.54 ± 0.55 sec^{-1}). This trend was not
165 observed in neurons from cultures prepared from Rab3A$^{Ebd/Ebd}$ mice, likely due to an increase in
166 frequency in untreated cells—frequencies remained high in TTX-treated cells (Figure 2H, CON,
167 1.71 ± 0.41 sec^{-1}; TTX, 3.05 ± 0.80 sec^{-1}).

168 Our results show that the homeostatic increase in mEPSC amplitude after activity
169 blockade is disrupted in both Rab3A$^{-/-}$ and the Rab3A$^{Ebd/Ebd}$ cortical neurons, strongly supporting
170 a crucial role of functioning Rab3A in this process. However, it is important to note that the
171 disruption differs for Rab3A$^{-/-}$ and Rab3A$^{Ebd/Ebd}$. In the Rab3A$^{-/-}$ data set, mEPSCs from untreated
172 cultures were indistinguishable from mEPSCs from Rab3A$^{+/+}$ untreated cultures, demonstrating
173 loss of Rab3A has no impact on basal activity mEPSC amplitudes, but the increase in mEPSC
174 amplitudes after activity blockade was strongly diminished in Rab3A$^{-/-}$ neurons. In the
175 Rab3A$^{Ebd/Ebd}$ data set, mEPSC amplitudes from untreated cultures were significantly larger than
176 those of untreated cultures from wild type mice, as can be seen comparing the CON values in
177 Figures 2E and F (CON, Rab3A$^{+/+}$, 11.0 ± 0.7 pA, vs. CON, Rab3A$^{Ebd/Ebd}$, 15.1 ± 1.0 pA, $p = 0.0027$,
178 Kruskal-Wallis test). The increase in mEPSC amplitude in cultures from Rab3A$^{Ebd/Ebd}$ mice is
179 consistent with the increase in mEPC amplitude we observed at the Rab3A$^{Ebd/Ebd}$ NMJ (Wang et
180 al., 2011). Similar increases in mEPSC amplitude at baseline, combined with a failure to increase
181 further after activity blockade, were noted in cultures prepared from mECP2, AKAP, Homer1a,

182 and Arc/Arg3.1 deletion mice (Shepherd et al., 2006; Hu et al., 2010; Xu and Pozzo-Miller, 2017;
183 Sanderson et al., 2018) as well as in cultures treated with ubiquitin proteasome inhibitors
184 (Jakawich et al., 2010a) or microRNA 186-5p (Silva et al., 2019), suggesting the possibility of a
185 generalized phenomenon in which increased mEPSC amplitude is induced when homeostatic
186 regulation is disrupted. Since we did not observe such an increase in mEPSC amplitude at
187 baseline in cultures from Rab3A$^{-/-}$ mice, it remains a possibility that the point mutant may bind
188 to novel partners, causing activities that would not be either facilitated or inhibited by Rab3A.
189 Still, it is a strong coincidence that the novel activity of the mutant Earlybird Rab3A would affect
190 mEPSC amplitude, the same characteristic that is modulated by activity blockade in a Rab3A
191 dependent manner. Finally, although we cannot rule out that once mEPSC amplitude is
192 increased at baseline, it is not possible for homeostatic plasticity to increase mEPSC amplitude
193 further due to a non-specific ceiling effect, the simplest interpretation is that the presence of
194 the mutant protein mimics the condition of activity blockade.
195 The small GTPase Rab3A is generally thought to function presynaptically to regulate
196 synaptic vesicle trafficking, possibly in an activity-dependent manner (Castillo et al., 1997;
197 Lonart et al., 1998; Leenders et al., 2001; Schluter et al., 2006; Coleman and Bykhovskaia, 2009;
198 Tian et al., 2012). In contrast, homeostatic plasticity of mEPSC amplitude has been attributed to
199 an increase in postsynaptic receptors on the surface of the dendrite (O'Brien et al., 1998;
200 Turrigiano et al., 1998). Is Rab3A required for the increase in surface AMPA-type glutamate
201 receptors that has been confirmed by multiple studies (see Introduction)? At the NMJ in vivo
202 we could find no evidence for an increase in AChRs after TTX block of the sciatic nerve in vivo
203 (Wang et al., 2005). The type of AMPA receptor that has been shown to be increased, calcium-

204 permeable GluA1-containing AMPA receptor or calcium-impermeable GluA2-containing AMPA
205 receptor, appears to depend on the experimental manipulation. For example, block of activity
206 by APV (NMDA antagonist) combined with TTX (inhibitor of Na^+ channels) induces an increase in
207 mEPSC amplitude in dissociated hippocampal cultures that is completely reversed by acute
208 application of the Ca^{2+}-permeable receptor-specific inhibitor NASPM (Sutton et al., 2006),
209 indicating the entirety of the homeostatic effect is due to an increase in homomeric Ca^{2+}-
210 permeable AMPA receptors, likely GluA1, although GluA3 and GluA4 are also Ca^{2+}-permeable
211 (Hollmann et al., 1991; Burnashev et al., 1992). Heteromeric receptors of any of these subunits
212 in combination with GluA2 would have rendered the receptors Ca^{2+}-impermeable and no longer
213 sensitive to NASPM (Blaschke et al., 1993; Bochet et al., 1994; Jonas and Burnashev, 1995). In
214 contrast, the increase in mEPSC amplitude in mouse hippocampal slice cultures induced by TTX
215 alone was not affected by another Ca^{2+}-permeable AMPA receptor inhibitor, philanthotoxin,
216 suggesting mediation by either GluA2-containing AMPA receptors or a presynaptic effect on
217 quantal size (Soden and Chen, 2010); see also, (Dubes et al., 2022).
218 Because we used TTX alone to block network activity, we expected that NASPM would
219 not reverse the TTX-induced increase in mEPSC amplitude in our mouse cortical cultures, and
220 we found that this was indeed the case. Figure 3A shows that the TTX-induced increase in mean
221 mEPSC amplitude was nearly identical in a set of 11 CON and 11 TTX-treated cells before and
222 after NASPM treatment (before NASPM, CON 12.9 ± 3.5 pA; TTX, 17.5 ± 3.1 pA; after NASPM,
223 CON 11.9 ± 2.6 pA; TTX 16.1 ± 3.5 pA). This result indicates that the TTX-induced increase in
224 mEPSC amplitude does not depend on Ca^{2+}-permeable receptors, since the effect of TTX clearly
225 remained when their presence was removed by acute NASPM application. We do not think that

226 there was any technical issue with the NASPM application, because overall, mEPSC amplitudes
227 were reduced modestly in both untreated and TTX-treated cultures (Figure 3B, CON, before
228 NASPM, 12.9 ± 3.5 pA; after, 11.9 ± 2.6 pA; TTX, before NASPM, 17.5 ± 3.1 pA; after, 16.1 ± 3.5
229 pA). Furthermore, NASPM consistently reduced mEPSC frequency (Figure 3C, CON, before
230 NASPM, 1.84 $\pm$ 0.55 sec^{-1}; after NASPM, 1.56 $\pm$ 0.53 sec^{-1}; TTX, before NASPM, 4.40 ± 3.51 sec^{-1};
231 after NASPM, 2.68 ± 2.25 sec^{-1}). Similar to the data in Figure 1, frequency is significantly
232 increased after TTX treatment ($p = 0.04$), but this difference is no longer significant after
233 NASPM application ($p = 0.20$). A loss in frequency after acute application of NASPM suggests
234 there are synaptic sites that express only homomers of Ca^{2+}-permeable receptors; mEPSCs from
235 these sites would be expected to be completely blocked by NASPM (see cartoon description in
236 Figure 3D, Left). The magnitude of the frequency reduction following acute NASPM appears to
237 be greater after TTX treatment, suggesting that loss of activity promotes the establishment of
238 synaptic sites that contain only Ca^{2+}-permeable receptors. However, these new sites do not
239 appear to contribute to the increase in mEPSC amplitude (Figure 3A). The lack of effect of
240 NASPM also rules out the contribution of Ca^{2+}-permeable forms of Kainate receptors GluA5 and
241 GluA6 (Koike et al., 1997; Sun et al., 2009).
242 Having established that homomeric Ca^{2+}-permeable receptors are not contributing to
243 the homeostatic increase in mEPSC amplitude, we turned to immunohistochemistry and
244 confocal imaging to assess whether GluA2 receptor expression, which will identify either GluA2
245 homomers or GluA1-GluA2 heteromers, was increased in our wild type mouse cortical cultures
246 following 48 hr treatment with TTX. Since mEPSCs necessarily report synaptic levels of
247 receptors, we used VGLUT1-immunofluorescence to identify synapses on pyramidal primary

248 apical dendrites labeled with MAP-2 immunofluorescence. We focused on the primary dendrite
249 of pyramidal neurons as a way to reduce variability that might arise from being at widely
250 ranging distances from the cell body, or, from inadvertently sampling dendritic regions arising
251 from other neurons, possibly inhibitory neurons. Figure 4 (Top) shows two pyramidal neurons,
252 one from an untreated culture on the left, and one from a TTX-treated culture on the right,
253 prepared from Rab3A$^{+/+}$ mice. To measure characteristics of synaptically located GluA2 receptor
254 clusters, we zoomed in on the primary dendrite (region in white rectangle). The zoomed regions
255 for single confocal sections of the selected area are shown below, and contain pairs of VGLUT1-
256 and GluA2-immunofluorescent clusters indicated by white trapezoidal frames. A dendrite
257 typically required ~10 confocal sections to be fully captured, and the total number of synaptic
258 pairs for all the sections imaged on a dendrite was usually < 20, so this is an atypically high
259 number of pairs within a single section; these particular dendrites and sections were selected
260 for illustration purposes. In addition to the synaptic pairs, we observed many GluA2-
261 immunofluorescent clusters not associated with VGLUT1 immunofluorescence (a few are
262 indicated with white arrows), most probably extrasynaptic receptors. There were also GluA2-
263 positive clusters present outside of MAP2-positive dendrites, which may be located on
264 astrocytes (Fan et al., 1999). Finally, GluA2 immunofluorescent clusters close to VGLUT1
265 immunofluorescence but not located along any apparent MAP2-positive neurites suggests the
266 presence of axon-axonal contacts, although VGLUT1 has also been detected in astrocytes
267 (Ormel et al., 2012). Only sites that contained both VGLUT1 and GluA2 immunofluorescence
268 close to the primary MAP2-postive dendrite or a secondary branch along this primary dendrite
269 were selected for analyses. In the experiment from which these images were collected, we

270 analyzed the distance from the cell body for each synapse. The average distance from the cell
271 body, for dendrites from the untreated cell, was 38.5 $\pm$ 2.8 μm; for the TTX-treated cell, it was
272 42.4 $\pm$ 3.2 μm ($p = 0.35$, Kruskal-Wallis test). Since the greatest distance from the cell body is
273 set by the outer limit of the zoom window, and that window was placed adjacent to the cell
274 body, distances in other experiments would be in this same range.

275 Variability in the magnitude of the homeostatic response from culture to culture is
276 averaged out in physiological experiments by the pooling of data from many cells across many
277 cultures. To reduce the necessity for many cultures, we chose to pair experiments in the same
278 cultures by recording mEPSCs from one set of coverslips, and processing another set of
279 coverslips from the same culture for immunofluorescence. We completed this matched
280 paradigm of physiology and immunofluorescence, which to our knowledge has never before
281 been done, for 3 cultures prepared from Rab3A$^{+/+}$ mice and 3 cultures prepared from Rab3A$^{-/-}$
282 mice. We present the results for mEPSC data and imaging data pooled across the 3 experiments
283 in Figure 5, with the data summarized in Table 1. Levels of GluA2 immunofluorescence at
284 synaptic sites were quantified by the size of the GluA2-immunofluorescent receptor cluster, the
285 average intensity value, and the integral of intensity values across the area of the cluster. In the
286 data pooled from the 3 matched experiments, neurons from Rab3A$^{+/+}$ cultures showed a
287 significant increase in mean mEPSC amplitudes following activity blockade (Figure 5A; Table 1).
288 This result indicates that the homeostatic response averaged across the 3 cultures was very
289 similar to, but slightly smaller than, that of the data set presented in Figure 1. The means for
290 size, intensity and integral of GluA2 immunofluorescent receptor clusters showed trends to
291 higher values after activity blockade, but the differences did not reach statistical significance

292 (Figure 5B size; Figure 5C intensity; Figure 5D integral; Table 1). These results support previous
293 studies demonstrating an increase in AMPA receptors following activity blockade, with the
294 magnitude of the changes in GluA2 receptor cluster size and integral matching that of mEPSC
295 amplitude, at around 20% (Table 1), but not achieving the same level of statistical significance.

296 As expected, mean mEPSC amplitude was not increased following activity blockade in
297 the data pooled from the new set of 3 Rab3A$^{-/-}$ cultures (Figure 5E). For immunofluorescence
298 results from the same Rab3A$^{-/-}$ cultures, no trend towards higher values was apparent for GluA2
299 receptor cluster characteristics (Figure 5F size; Figure 5G intensity; Figure 5H integral; Table 1).
300 Taken together, these results indicate that the modest increases in GluA2 receptor cluster size
301 and integral following activity blockade observed in wild-type cultures do not occur in the
302 absence of Rab3A. These results suggest the surprising finding that the presynaptic vesicle
303 protein Rab3A is involved in the regulation of postsynaptic AMPA receptors during homeostatic
304 plasticity.

305 As noted above, the homeostatic increase in mEPSC amplitude in cultures from Rab3A$^{+/+}$
306 mice reached significance whereas that of receptor levels did not. To determine where this
307 disparity was coming from, we compared mEPSC amplitude and GluA2 receptor data within
308 individual experiments. In order to evaluate whether a particular culture displayed homeostatic
309 plasticity of mEPSC amplitude, we set a minimum requirement of recording from 6 cells per
310 condition, meaning a successful experiment required at least 12 usable recordings in one day (6
311 CON and 6 TTX; i.e. low holding current, stable baseline, low noise, etc.). Ultimately, our sample
312 size ranged from 6 to 10 cells per condition per culture. Figures 6A-C show the box plots for
313 mEPSC amplitudes, and GluA2 receptor cluster size, intensity and integrals, for 3 individual

314 Rab3A$^{+/+}$ cultures. With these small sample sizes, the differences between untreated and TTX-
315 treated cells were not statistically significant for mEPSC amplitudes in any of the 3 cultures, but
316 an upward trend occurred in every case, ranging from 12 to 28% (Table 1). Second, in two of
317 the three Rab3A$^{+/+}$ experiments (Cultures #1 and #2) GluA2 receptor cluster size increased 22
318 and 56%, respectively, significantly so for Culture #2 (Table 1). However, in one experiment
319 (Culture #3), GluA2 receptor cluster size showed a downward trend of 9.5%. Because we have
320 10 CON mean mEPSC amplitudes and 9 TTX mean mEPSC amplitudes that indicate this
321 particular culture very likely has a normal homeostatic increase in mEPSC amplitude induced by
322 activity blockade, the lack of increase in GluA2 receptor cluster characteristics suggests that
323 mEPSC amplitudes can increase in the absence of an increase in receptors. Furthermore,
324 Culture #3's opposite results from Cultures #1 and #2, explain why in the pooled data set, the
325 increase in GluA2 receptor characteristics after TTX treatment do not reach statistical
326 significance.

327 Figures 7A-C show the box plots for mEPSC amplitudes, and GluA2 receptor cluster size,
328 intensity and integrals, for 3 individual Rab3A$^{-/-}$ cultures. Here, mEPSC amplitudes showed a
329 downward trend in all 3 cultures, as did GluA2 receptor characteristics for two of the three
330 cultures. But we found another obvious mismatch between the mEPSC amplitude data and the
331 GluA2 receptor cluster data for one of the Rab3A$^{-/-}$ cultures. For Culture #3 (Figure 7C), the box
332 plot of mEPSC mean amplitudes showed a downward trend after TTX treatment, decreasing by
333 7% (Table 1), whereas GluA2 receptor cluster size, intensity and integral all showed upward
334 trends, the increase ranging from 6 to 23% (Table 1). This result may suggest that the disruption
335 of the homeostatic increase in receptors in the absence of Rab3A is not absolute. It also

336 indicates that synaptic GluA2 receptor levels can increase without an accompanying increase in
337 mEPSC amplitudes.

338 In summary, our matched mEPSC and receptor cluster results indicate that: 1. activity
339 blockade resulted in an increase in mEPSC amplitudes usually accompanied by an increase in
340 synaptic GluA2 receptors; 2. loss of Rab3A disrupted both the increase in mEPSC amplitudes
341 and the increase in GluA2 receptor levels; and 3. The differences between homeostatic
342 responses of mEPSC amplitudes and the GluA2 cluster sizes within the same cultures suggest
343 there may be other factors that contribute to mEPSC amplitude.

344 Having used VGLUT1 immunofluorescence to mark synaptic sites, we could also ask
345 whether there was a presynaptic effect of activity blockade on the size, intensity or integral of
346 the VGLUT1 signal at sites apposed to the previously examined GluA2 postsynaptic sites. In the
347 pooled data from cultures prepared from Rab3A$^{+/+}$ mice, we found no change in the size of the
348 VGLUT1-positive regions, and trends towards reduced intensity and integral (Table 2). These
349 data do not support the idea that activity blockade caused an increase in the amount of
350 VGLUT1 per vesicle, although we cannot rule out that a simultaneous reduction in the number
351 of vesicles obscured the effect, since we did not have an independent label for synaptic
352 vesicles. In cultures prepared from Rab3A$^{-/-}$ mice, the size, intensity and integral of the VGLUT1-
353 positive regions showed upward trends (Table 2), suggesting the possibility that the modest
354 decreases observed for cultures prepared from wild type mice depend on Rab3A, but it is
355 difficult to make any conclusions when the p values are far from reaching significance. Similarly
356 to the GluA2 receptor cluster data, the likely reason that the pooled data effects did not reach
357 significance is because the effects were not consistent across all three cultures, with one

358 Rab3A$^{+/+}$ culture showing an upward trend instead of a downward trend, and one Rab3A$^{-/-}$
359 culture showing a downward trend instead of an upward trend (Table 2). It should be noted
360 that there was no consistent inverse pattern for GluA2 vs. VGLUT1. While in cultures prepared
361 from Rab3A$^{-/-}$ mice, when GluA2 characteristics trended downward, VGLUT1 characteristics
362 trended upward, this pattern did not hold for cultures prepared from Rab3A$^{+/+}$ mice. In
363 Rab3A$^{+/+}$ Culture #2, GluA2 showed significant increases, and VGLUT1 showed essentially no
364 change. In Rab3A$^{+/+}$ Culture #3, both GluA2 and VGLUT1 trended downwards. Taken together,
365 the GluA2 and VGLUT1 immunofluorescence data indicate that GluA2 receptors likely
366 contribute to the increase in mEPSC amplitudes after activity blockade in Rab3A$^{+/+}$ cultures, and
367 the disruption of that increase in Rab3A$^{-/-}$ cultures, but VGLUT1 levels change in the opposite
368 direction from mEPSC amplitudes. Interestingly, VGLUT1 levels are strongly affected by loss of
369 Rab3A, with a highly significant decrease in integral in untreated cultures from Rab3A$^{-/-}$ mice,
370 compared to untreated cultures from Rab3A$^{+/+}$ mice (size, $p = 0.019$; intensity, $p = 0.004$;
371 integral, $p = 4.6 * 10^{-4}$; Table 2).
372 We have demonstrated here for the first time that the synaptic vesicle protein Rab3A
373 influences the homeostatic regulation of postsynaptic GluA2 receptors. What are possible ways
374 that Rab3A could exert a postsynaptic action? It has previously been shown that exogenous
375 addition of TNFα to hippocampal cultures causes an increase in surface expression of GluA1
376 receptors (although not GluA2 receptors), and that the homeostatic increase in mEPSC
377 amplitudes is abolished in cultures prepared from the TNFα deletion mouse (Stellwagen et al.,
378 2005; Stellwagen and Malenka, 2006). Furthermore, neurons from TNF$\alpha^{+/+}$ mice plated on glial
379 feeder layers derived from TNF$\alpha^{-/-}$ mice fail to show the increase in mEPSC amplitude after TTX

380 treatment, indicating that the TNFα inducing the receptor increases following activity blockade
381 comes from the glial cells (Stellwagen and Malenka, 2006). It has recently been shown that the
382 source of TNFα is astrocytes rather than microglia (Heir et al., 2024). Rab3A has been detected
383 in astrocytes (Maienschein et al., 1999; Hong et al., 2016), so to determine whether Rab3A is
384 acting via regulating TNFα release from astrocytes, we performed experiments similar to those
385 of Stellwagen and Malenka (2006) (schema illustrated in Figure 8, Left). It should be noted that
386 under our culturing conditions, the glial feeder layers would be expected to be composed
387 mainly of astrocytes (Heir et al., 2024). We compared the effect of activity blockade on mEPSC
388 amplitudes recorded from cortical neurons from Rab3A$^{+/+}$ mice plated on Rab3A$^{+/+}$ glial feeder
389 layers (Figure 8A); neurons from Rab3A$^{+/+}$ mice plated on Rab3A$^{-/-}$ glia (Figure 8B), and neurons
390 from Rab3A$^{-/-}$ mice plated on Rab3A$^{+/+}$ glia (Figure 8C). If Rab3A is required for TNFα release
391 from glia, then Rab3A$^{+/+}$ neurons plated on Rab3A$^{-/-}$ glia should not show a homeostatic
392 increase in mEPSC amplitude after treatment with TTX, and any cultures with Rab3A$^{+/+}$ glia
393 should have a normal homeostatic response. We found the opposite result: mEPSC amplitudes
394 increased dramatically in cultures where Rab3A was present in neurons (WT on WT, CON, 13.3
395 $\pm$ 0.5 pA, TTX, 16.7 $\pm$ 1.2 pA; WT on KO, CON, 13.3 $\pm$ 1.0 pA, TTX, 18.8 $\pm$ 1.4 pA), but the
396 increase was greatly diminished in cultures where Rab3A was present only in glia (KO on WT,
397 CON, 15.2 $\pm$ 1.1 pA, TTX, 16.9 $\pm$ 0.7 pA). It is interesting to note that in the glial feeder layer
398 culture, the loss of Rab3A in the neurons may have caused an increase in mEPSC amplitude at
399 baseline, similar to the Earlybird mutant in dissociated cultures, but it is also possible this can
400 be attributed to culture to culture variability. Regarding mEPSC frequency, in cultures with
401 Rab3A$^{+/+}$ neurons, frequency trended upward after activity blockade, whereas in the culture

402 with Rab3A$^{-/-}$ neurons, frequency was already increased, and trended downward after activity
403 blockade.

404 In summary, in the absence of Rab3A from glia, the homeostatic plasticity of mEPSC
405 amplitude following activity blockade was completely normal, whereas in the absence of Rab3A
406 in neurons, homeostatic plasticity was greatly diminished. This result makes it highly unlikely
407 that Rab3A is required for the release of TNFα, or another factor from glia, that induces a
408 homeostatic upregulation of postsynaptic receptors and thereby increases mEPSC amplitude
409 following TTX treatment. Neuronal Rab3A appears to mediate the homeostatic increase in
410 mEPSC amplitude following activity blockade.

411

412 Discussion

413 We found that homeostatic synaptic plasticity of mEPSC amplitude in dissociated mixed
414 cultures of mouse cortical neurons and glia behaved remarkably similar to the mouse NMJ in
415 response to loss of Rab3A function: in cultures from Rab3A$^{-/-}$ mice, the increase in mEPSC
416 amplitudes following prolonged network silencing by TTX was strongly diminished, and in
417 cultures from Rab3A$^{Ebd/Ebd}$ mice, basal mEPSC amplitude was increased compared to that of
418 wild-type cultures and was not further modified by TTX treatment. These results suggest that
419 normal function of the synaptic vesicle protein Rab3A is required for the homeostatic increase
420 of mEPSC amplitude in cortical cultures. The effect of TTX on mEPSC amplitude was not due to
421 increases in Ca^{2+}-permeable homomers because acute NASPM application was unable to
422 reverse the increase in amplitude after TTX treatment. We used imaging of

423 immunofluorescence to demonstrate a strong trend towards increased GluA2 levels at synapses
424 in activity-blocked cultures from Rab3A$^{+/+}$ mice that was no longer apparent in the absence of
425 Rab3A, suggesting the surprising idea that this protein, previously implicated primarily in the
426 regulation of calcium-dependent vesicle fusion, is also important for the regulation of surface
427 expression of postsynaptic receptors. We found a significant increase in mEPSC frequency after
428 activity blockade that was no longer significant in the absence of Rab3A, which was less
429 surprising as frequency is known to depend on presynaptic factors. At the neuromuscular
430 junction, higher mEPC frequencies that occur in 0.5 mM extracellular calcium and above were
431 significantly reduced in the Rab3A deletion mouse (Coleman et al., 2007). On the other hand,
432 the increase in frequency after TTX treatment is also strongly diminished after acute application
433 of NASPM, suggesting there may be an increase in the number of synapses with only Ca^{2+}-
434 permeable homomers. It remains to be determined if this effect is Rab3A-dependent or if there
435 are two distinct mechanisms contributing to homeostatic plasticity of frequency.

436 The levels of the glutamate transporter, VGLUT1, were not increased after activity
437 blockade under our experimental conditions. A similar lack of increase in VGLUT1 levels,
438 relative to synapsin in imaging of immunofluorescence, was previously observed in
439 hippocampal cultures treated with NBQX, an AMPA receptor blocker (see supplemental data,
440 (Wilson et al., 2005)). On the other hand, treatment with AP5, an NMDA receptor blocker, was
441 able to induce an increase in VGLUT1 levels relative to synapsin (Wilson et al., 2005), suggesting
442 that this presynaptic response depends on the type of activity manipulation. Another study
443 showed increased VGLUT1 mRNA and protein in western blots in cortical cultures treated with
444 TTX, but only examined VGLUT1 at synapses using imaging following treatment with bicuculline

445 (De Gois et al., 2005). Taken together with our findings, it appears that there is not strong
446 evidence that the amount of VGLUT1 at synapses is a contributing factor to the increase in
447 mEPSC amplitude after activity blockade with TTX.

448 *Homeostatic plasticity of postsynaptic receptors was less consistent than that of mEPSC*
449 *amplitude*

450 While we found that the effect of TTX treatment on mEPSC amplitude and GluA2
451 receptor levels were of very similar magnitude, the effect on GluA2 receptor levels was not
452 statistically significant for the pooled data sets acquired in the same cultures. We determined
453 that this discrepancy was due to one of the three cultures showing a downward trend in GluA2
454 receptor levels after activity blockade. In light of the extensive literature documenting increases
455 in GluA1 or GluA2 receptors, or both, after activity blockade, the less than convincing increase
456 in GluA2 receptor levels in the current work came as a surprise. Therefore we reviewed what
457 has previously been shown, and were able to identify only 5 studies that examined the effect of
458 activity blockade using TTX alone, reported levels of AMPA receptors specifically localized to
459 synapses, and recorded mEPSCs in the same study, although not in the same cultures (Hou et
460 al., 2008; Ibata et al., 2008; Jakawich et al., 2010a; Xu and Pozzo-Miller, 2017; Dubes et al.,
461 2022). Since our issue is not with the magnitude of the changes being different for receptors
462 and mEPSC amplitudes, but with statistical significance (or consistency) being different between
463 the two methods, we wanted to determine whether the previous studies showed any evidence
464 of greater variability in receptor measurements. Only a single study had comparable sample
465 sizes for receptors and mEPSC amplitudes (either because number of receptor sites is used
466 instead of cells, or because the number of cells differs for the two types of experiments), and

467 the p value was < 0.01 for mEPSC amplitudes (n = 9 and 10 cells for CON and TTX, respectively),
468 but < 0.05 for receptor data (n = 13 and 14 cells for CON and TTX) (Xu and Pozzo-Miller, 2017).
469 This single example is consistent with the idea that the receptor data are more variable than
470 mEPSC data. Even if a difference in consistency could be established in multiple studies, it
471 remains a possibility that the disparity is attributable to the unique limitations of the two types
472 of experiments. Nevertheless, the finding that mEPSC amplitude can increase despite a
473 decrease in receptors suggests receptors may not be the only contributor to the TTX effect on
474 mEPSC amplitude.
475
476 *Neuronal, not glial, Rab3A may be required for the homeostatic release of a signaling molecule*
477 Our results support the surprising possibility that the presynaptic vesicle protein Rab3A
478 regulates postsynaptic AMPARs. Astrocytic release of TNFα was shown to mediate the increase
479 in mEPSC amplitudes in prolonged TTX-treated cultures of dissociated hippocampal neurons
480 and cultures of hippocampal slices (Stellwagen and Malenka, 2006; Heir et al., 2024), but we
481 found that loss of Rab3A in glia did not disrupt the increase in mEPSC amplitude after activity
482 blockade. Further, we previously showed that the homeostatic increase in NMJ mEPC
483 amplitude was completely normal in the absence of TNFα (Wang et al., 2011). This leaves
484 neuronal Rab3A as the potential controller of a soluble factor regulating surface expression of
485 receptors.
486 One possible signaling molecule being controlled by Rab3A is brain-derived
487 neurotrophic factor (BDNF). Addition of exogenous BDNF to neuronal cultures prevents the
488 increase in mEPSC amplitude following activity blockade (Rutherford et al., 1998; Benevento et

489 al., 2016) but see (Smith-Dijak et al., 2019), and BDNF mRNA is reduced after activity blockade
490 in vitro (Benevento et al., 2016; Miyasaka and Yamamoto, 2021) and in vivo (Castren et al.,
491 1992). Also, after reduction of secreted BDNF in culture media via the BDNF scavengers TrkB-FC
492 or TrkB-IgG, mEPSC amplitudes are increased (Rutherford et al., 1998; Benevento et al., 2016;
493 Smith-Dijak et al., 2019). Reduction of Rab3A in astrocytes decreases astrocytic BDNF release
494 (Hong et al., 2016). Taken together, these studies suggest that activity blockade could cause a
495 Rab3A-dependent inhibition of BDNF release, leading to an increase in postsynaptic receptors.
496 However, we have no evidence that Rab3A is required for the regulation of BDNF release from
497 neurons, so it is just as likely that after activity blockade, Rab3A acts in a positive way to
498 promote release of a trophic molecule that stimulates the insertion of postsynaptic receptors. It
499 is unlikely that Rab3A is required when activity is normal because receptor levels do not change
500 in the same way with loss of Rab3A as they do with loss of activity. Rather, our data fit with a
501 model in which Rab3A mainly becomes engaged in response to activity blockade (Figure 9).
502
503 *Is Rab3A acting in the postsynaptic cell to cause homeostatic increase in mEPSC amplitude?*
504 To our knowledge, there is no evidence localizing Rab3A to postsynaptic sites. Other
505 presynaptic molecules, such as SNARE proteins, synaptotagmins, and NSF, have been identified
506 in the postsynaptic compartment (Lledo et al., 1998; Nishimune et al., 1998; Osten et al., 1998;
507 Song et al., 1998; Araki et al., 2010; Kennedy et al., 2010; Suh et al., 2010; Jurado et al., 2013;
508 Hussain and Davanger, 2015; Gu et al., 2016; Wu et al., 2017) but Rab3A localization was not
509 examined in those studies. On the other hand, a recent report implicates Rab3A in the
510 localization of plasma membrane proteins in rafts in HEK cells and Jurkat-T cells, indicating

511 Rab3A can be found in locations other than the presynaptic nerve terminal (Diaz-Rohrer et al.,
512 2023). In this study a reduction in all Rab3 isoforms led to an impairment of plasma membrane
513 localization of epidermal growth factor receptor (EGFR), so it is possible that Rab3A is acting
514 similarly in postsynaptic dendrites to promote transport of GluA2 receptors to the surface after
515 activity blockade (Figure 9). Another possibility, not depicted in Figure 9, is that Rab3A acts
516 postsynaptically to regulate the release of a trophic factor that in turn regulates surface
517 expression of GluA2 receptors. This idea is consistent with evidence that BDNF is synthesized
518 and released locally from dendrites (Jakawich et al., 2010b; Thapliyal et al., 2022).
519

520 *Alternate contributors to homeostatic increase in mEPSC amplitude*

521 We do not think Rab3A impacts homeostatic synaptic plasticity solely through pre- or
522 postsynaptic regulation of GluA2 receptor trafficking to the plasma membrane. First, prolonged
523 activity blockade with TTX at the NMJ led to an increase in mEPC amplitude that was not
524 accompanied by any increase in AChR levels, yet it was dependent on Rab3A (Wang et al.,
525 2011). Second, mEPSC amplitudes increased in three cortical cultures treated with TTX, but
526 GluA2 receptor levels in one of the cultures actually went down. An increase in conductance
527 could explain the increase in mEPSC amplitudes in the absence of receptor level increases, but
528 all evidence to date suggests that the only way to increase conductance is to either switch from
529 GluA2-containing heteromeric receptors to GluA1 homomers, which have much greater
530 conductance (Oh and Derkach, 2005; Soares et al., 2013; Hou et al., 2015; Xu and Pozzo-Miller,
531 2017; Benke and Traynelis, 2019; Silva et al., 2019; Dubes et al., 2022), or, to post-
532 translationally modify the receptor. Such conductance-altering modifications have been

533 demonstrated only for GluA1 (Derkach et al., 1999; Kristensen et al., 2011; Jenkins and
534 Traynelis, 2012). Importantly, any change in conductance due to an increase in GluA1
535 homomers or modification of GluA1 should have been detected by NASPM being able to
536 disrupt the homeostatic increase in mEPSC amplitude, and this was not what we observed.
537 The other contributor to mEPSC amplitude besides receptors is the size of the
538 presynaptic quantum, or the amount of transmitter released during a single fusion event. As
539 stated above, we found a downward trend in VGLUT1 levels after activity blockade. This
540 downward trend was not apparent in cultures prepared from Rab3A$^{-/-}$ mice, suggesting a
541 possible Rab3A-dependent effect. Interestingly, Rab3A levels are reduced 50% in hippocampal
542 extracts from mice lacking VGLUT1 (Fremeau et al., 2004). Coupled with our finding that loss of
543 Rab3A was associated with a highly significant decrease in VGLUT1 levels in untreated cultures,
544 these results suggest an interdependence between Rab3A and VGLUT1. More importantly, our
545 results rule out VGLUT1 levels as the source for increased mEPSC amplitude.
546 The amount of transmitter released during vesicle fusion can be affected by the kinetics
547 of the fusion pore opening (Chang et al., 2017). We previously used amperometric
548 measurements in mouse adrenal chromaffin cells to show loss of Rab3A increased the
549 occurrence of very small amplitude fusion pore feet (Wang et al., 2008). Paired with our finding
550 that there is an increase in the occurrence of very slow-rising, abnormally shaped mEPCs at the
551 neuromuscular junction of Rab3A$^{-/-}$ mice, our data suggest that small synaptic vesicles may
552 have a fusion pore step under certain circumstances (see also (Chiang et al., 2018)). If activity
553 blockade causes an increase in mEPSC amplitude due to a more rapid opening of a fusion pore,
554 or a larger fusion pore conductance, it is possible that Rab3A is required for this modulation.

555 Finally, a simple way to increase the amount of transmitter released by a vesicle is to
556 enlarge vesicle size. Larger vesicle diameter has been observed following activity disruption in
557 multiple paradigms, including ocular deprivation, cortical ablation, and immobilization (Kawana
558 et al., 1971; Lloret and Saavedra, 1975; Cheresharov et al., 1978). Loss of Rab3 family members
559 is associated with increased vesicle size (Riedel et al., 2002; Schonn et al., 2010). Finally, an
560 increase in volume has been shown to increase miniature endplate junctional current
561 amplitude at the Drosophila NMJ (Karunanithi et al., 2002). Rab3A could be required for an
562 activity-dependent increase in vesicle size, but the increase in diameter needed for a 25%
563 increase in transmitter, and therefore mEPSC amplitude, would be difficult to detect.

564 To our knowledge, this is the first evidence of a presynaptic protein being implicated in
565 the homeostatic regulation of mEPSC amplitude and AMPARs in neuronal cultures. Homeostatic
566 synaptic plasticity is becoming increasingly implicated in essential normal functions such as
567 sleep (Tononi and Cirelli, 2014; Diering et al., 2017; Torrado Pacheco et al., 2021), and
568 pathological conditions such as epilepsy, neuropsychiatric disorders, Huntington's, and alcohol
569 use disorder (Trasande and Ramirez, 2007; Fernandes and Carvalho, 2016; Wang et al., 2017;
570 Lovinger and Abrahao, 2018; Smith-Dijak et al., 2019; Lignani et al., 2020; Suzuki et al., 2021;
571 Kavalali and Monteggia, 2023). Therefore our identification of a novel regulatory pathway
572 involving Rab3A may have important therapeutic implications. In future work it will be
573 important to determine whether Rab3A is acting presynaptically or postsynaptically to regulate
574 GluA2 receptors, and what other contributor to mEPSC amplitude depends on Rab3A, possibly
575 fusion pore characteristics or vesicle volume.

576

577 Materials and Methods

578 *Animals.* To determine the role of Rab3A in homeostatic plasticity in mouse cortical cultures,
579 we employed two distinct genetic mouse strains with altered Rab3A function. Rab3A deletion
580 mice were generated as follows: Rab3A$^{+/-}$ heterozygous mice were bred and genotyped as
581 previously described (Kapfhamer et al., 2002; Wang et al., 2008), and maintained as a colony
582 using multiple heterozygous breeding pairs. Homozygous Rab3A$^{+/+}$ or Rab3A$^{-/-}$ mouse pups
583 were obtained by breeding Rab3A$^{+/+}$ pairs and Rab3A$^{-/-}$ pairs, respectively, so that the pups
584 were the first generation progeny of a homozygous mating. This protocol minimizes the
585 tendency of multiple generations of Rab3A$^{+/+}$ and Rab3A$^{-/-}$ homozygous breedings to produce
586 progeny that are more and more genetically distinct. Rab3A$^{Ebd/Ebd}$ mice were identified in an
587 EU-mutagenesis screen of C57BL/6J mice, and after a cross to C3H/HeJ, were backcrossed for 3
588 generations to C57BL/6J (Kapfhamer et al., 2002). Rab3A$^{+/Ebd}$ heterozygous mice were bred at
589 Wright State University and genotyped in a two-step procedure: 1. a PCR reaction (forward
590 primer: TGA CTC CTT CAC TCC AGC CT; reverse primer: TGC ACT GCA TTA AAT GAC TCC T)
591 followed by 2. a restriction digest with enzyme Bsp1286I (New England Biolabs) that
592 distinguishes the Earlybird mutant by its different base-pair products. Rab3A$^{+/-}$ mice were
593 backcrossed with Rab3A$^{+/+}$ mice from the Earlybird heterozygous colony for 11 generations in
594 an attempt to establish a single wild type strain, but differences in mEPSC amplitude and
595 adrenal chromaffin cell calcium currents persisted, likely due to genes that are close to the
596 Rab3A site, resulting in two wild type strains: 1. Rab3A$^{+/+}$ from the Rab3A$^{+/-}$ colony, and 2.
597 Rab3A$^{+/+}$ from the Rab3A$^{+/Ebd}$ colony.

598 *Primary Culture of Mouse Cortical Neurons.* Primary dissociated cultures of mixed neuronal and
599 glia populations were prepared as previously described (Hanes et al., 2020). Briefly, postnatal
600 day 0-2 (P0-P2) Rab3A$^{+/+}$, Rab3A$^{-/-}$ or Rab3A$^{Ebd/Ebd}$ neonates were euthanized by rapid
601 decapitation, as approved by the Wright State University Institutional Animal Care and Use
602 Committee, and brains were quickly removed. Each culture was prepared from the cortices
603 harvested from two animals; neonates were not sexed. Cortices were collected in chilled
604 Neurobasal-A media (Gibco) with osmolarity adjusted to 270 mOsm and supplemented with 40
605 U/ml DNAse I (ThermoFisher Scientific). The tissues were digested with papain (Worthington
606 Biochemical) at 20 U/ml at 37°C for 20 minutes followed by trituration with a sterile, fire-
607 polished Pasteur pipette, then filtered through a 100 μm cell strainer, and centrifuged at 1100
608 rpm for 2 minutes. After discarding the supernatant, the pellet was resuspended in room
609 temperature Neurobasal-A media (270 mOsm), supplemented with 5% fetal bovine serum for
610 glia growth, and 2% B-27 supplement to promote neuronal growth (Gibco), L-glutamine, and
611 gentamicin (ThermoFisher Scientific). Neurons were counted and plated at 0.15 * 10^6
612 cells/coverslip onto 12 mm coverslips pre-coated with poly-L-lysine (BioCoat, Corning). This
613 plating density produces a "high density" culture characterized by a complex mesh of neuronal
614 processes criss-crossing the field of view, completely filling the space between cell bodies (see
615 Figure 4). We found in preliminary experiments that an increase in mEPSC amplitude in mouse
616 cortical cultures was inconsistent when cell density was low, likely due to lower levels of
617 baseline activity, although it is a limitation of this study that we did not directly measure activity
618 levels in cultures prepared from Rab3A$^{+/+}$, Rab3A$^{-/-}$ or Rab3A$^{Ebd/Ebd}$ mice, and therefore do not
619 know if differences in results are due to differences in activity levels. While unlikely for Rab3A$^{+/+}$

620 and Rab3A$^{-/-}$ studies, given the mEPSC amplitude in untreated cultures that was relatively small,
621 it remains possible that in Rab3A$^{Ebd/Ebd}$ studies, the larger mEPSC amplitude in untreated
622 cultures was due to a loss of activity in these cultures. The culture media for the first day (0 DIV)
623 was the same as the above Neurobasal-A media supplemented with FBS, B-27, L-glutamine, and
624 gentamicin, and was switched after 24 hours (1 DIV) to media consisting of Neurobasal-A (270
625 mOsm), 2% B-27, and L-glutamine without FBS to avoid its toxic effects on neuronal viability
626 and health (Stellwagen and Malenka, 2006). Half of the media was changed twice weekly and
627 experiments were performed at 13-14 DIV. Two days prior to experiments, tetrodotoxin (TTX)
628 (500 nM; Tocris), a potent Na^+ channel blocker, was added to some cultures to chronically
629 silence all network activity and induce homeostatic synaptic plasticity mechanisms, while
630 untreated sister cultures served as controls. Cultures prepared from mutant mice were
631 compared with cultures from wild-type mice from their respective colonies. Note that the
632 cultures comprising the Rab3A$^{+/+}$ data here are a subset of the data previously published in
633 Hanes et al., 2020. This smaller data set was restricted to the time period over which cultures
634 were also prepared from Rab3A$^{-/-}$ mice.

635 *Preparation of Glial Feeder Layers.* Glial feeder layers were prepared from the cortices of P0-P2
636 Rab3A$^{+/+}$ or Rab3A$^{-/-}$ mouse pups as described previously (Stellwagen and Malenka, 2006).
637 Briefly, cortices were dissected and cells were dissociated as described above. Cell suspensions
638 of mixed neuronal and glial populations were plated onto glass coverslips pre-coated with poly-
639 L-lysine in Dulbecco's Modified Eagle Media (ThermoFisher Scientific) supplemented with 5%
640 FBS (to promote glial proliferation and to kill neurons), L-glutamine, and gentamicin, and
641 maintained in an incubator at 37°C, 5% CO_2; cultures were maintained in this manner for up to

642 1 month to generate purely glial cultures (all neurons typically died off by 7 DIV). Culture media
643 was replaced after 24 hours, and subsequent media changes were made twice weekly,
644 replacing half of the culture media with fresh media. Feeder layers were not used for neuronal
645 seeding until all native neurons were gone and glia approached 100% confluency (visually
646 inspected).

647 *Plating of Neurons on Glial Feeder Layers.* Cortical neurons were obtained as described above.
648 The cell pellet obtained was resuspended in Neurobasal-A (osmolarity adjusted to 270 mOsm)
649 containing B27 (2%, to promote neuronal growth), L-glutamine, and 5-fluorodeoxyuridine (FdU,
650 a mitotic inhibitor; Sigma). Addition of FdU was used to prevent glial proliferation and
651 contamination of the feeder layer with new glia, promoting only neuronal growth on the feeder
652 layers (FdU-containing media was used for the maintenance of these cultures and all
653 subsequent media changes). Glial culture media was removed from the feeder layer cultures,
654 and the neuronal cell suspension was plated onto the glial feeder cultures. The culture strategy
655 used to distinguish the relative roles of neuronal and glial Rab3A is outlined in Figure 8, Left. At
656 1 DIV, all of the culture media was removed and replaced with fresh Neurobasal-A media
657 containing FdU described above, and half of the media was replaced twice per week for all
658 subsequent media changes. Cultures were maintained in a 37°C, 5% CO_2 incubator for 13-14
659 DIV.

660 *Whole-Cell Voltage Clamp to Record mEPSCs*. At 13-14 DIV, mEPSCs from TTX-treated and
661 untreated sister cultures of Rab3A$^{+/+}$ or Rab3A$^{-/-}$ neurons from the Rab3A$^{+/-}$ colony, or Rab3A$^{+/+}$
662 or Rab3A$^{Ebd/Ebd}$ neurons from the Rab3A$^{+/Ebd}$ colony, were recorded via whole-cell voltage clamp
663 to assess the role of Rab3A in homeostatic synaptic plasticity. Recordings were taken from

664 pyramidal neurons, which were identified visually by a prominent apical dendrite; images were
665 taken of all cells recorded from. Cells were continuously perfused with a solution consisting of
666 (in mM): NaCl (115), KCl (5), $CaCl_2$ (2.5), $MgCl_2$ (1.3), dextrose (23), sucrose (26), HEPES (4.2),
667 pH = 7.2 (Stellwagen and Malenka, 2006). On the day of recording, the osmolarity of the media
668 from the cultures was measured (normally 285 – 295 mOsm) and the perfusate osmolarity was
669 adjusted to match the culture osmolarity, to protect against osmotic shock to the neurons. To
670 isolate glutamatergic mEPSCs, TTX (500 nM) and picrotoxin (50 μM) were included in the
671 perfusion solution to block action potentials and GABAergic currents, respectively. The NMDA
672 receptor antagonist, APV, was not included in the perfusion solution because in pilot studies, all
673 mEPSCs were blocked by 10 μM CNQX and 50 μm picrotoxin, demonstrating no APV-sensitive
674 mEPSCs were present (data not shown). Previous studies have described NMDA mEPSCs in
675 neuronal cultures, but recordings were performed in 0 Mg^{2+} (Watt et al., 2000; Sutton et al.,
676 2006). In our recordings, the presence of extracellular Mg^{2+} (1.3 mM) <u>and</u> TTX would mean that
677 the majority of NMDA receptors are blocked by extracellular Mg^{2+} at resting Vm. Patch
678 electrodes (3.5 – 5 MΩ) were filled with an internal solution containing (in mM): K-gluconate
679 (130), NaCl (10), EGTA (1), $CaCl_2$ (0.132), $MgCl_2$ (2), HEPES (10), pH = 7.2. Osmolarity was
680 adjusted to 10 mOsm less than the perfusion solution osmolarity, which we have found
681 improves success rate of achieving low access resistance recordings. Neurons were clamped at
682 a voltage of -60 mV using an Axopatch 200B patch-clamp (Axon Instruments), recorded from for
683 2 – 5 minutes, and data were collected with Clampex 10.0/10.2 (Axon Instruments).
684

685 *NASPM application*. The antagonist of Ca^{2+}-permeable AMPA receptors, N-naphthyl
686 acetylspermine (NASPM, 20 μM; Tocris), was applied during recordings in a subset of
687 experiments. NASPM is a synthetic analog of Joro Spider Toxin (JSTX) (Koike et al., 1997), and
688 chemicals in this family block Ca^{2+} permeable glutamate receptors (Blaschke et al., 1993;
689 Herlitze et al., 1993; Iino et al., 1996). The presence of the edited GluA2 subunit disrupts both
690 the Ca^{2+} permeability and the sensitivity to JSTX and related substances (Blaschke et al., 1993;
691 Bochet et al., 1994; Jonas and Burnashev, 1995). Therefore, 20 μM NASPM is expected to
692 completely block AMPA receptors containing GluA1, GluA3 or GluA4 subunits (Hollmann et al.,
693 1991; Burnashev et al., 1992), or the Kainate receptors containing GluA5 or GluA6 (Koike et al.,
694 1997; Sun et al., 2009), but be ineffective against any heteromer or homomer containing GluA2
695 subunits. Because the effect of the spider toxins and their analogues are use-dependent
696 (Herlitze et al., 1993; Iino et al., 1996; Koike et al., 1997), NASPM was applied with a mildly
697 depolarizing high K^+ solution (25 mM KCl, 95 mM NaCl) which we expected to trigger release of
698 glutamate and opening of glutamate-activated receptors, allowing entry of the pore blocker.
699 Baseline recordings were performed for 2 minutes in our standard perfusate, then were
700 suspended while NASPM + High K^+ solution was applied for 45 seconds, followed by a NASPM
701 only solution for 5 minutes, after which recording was recommenced for 5 minutes (because
702 we found in pilot experiments that frequency was reduced following NASPM application).
703 *Analysis of mEPSCs.* Miniature excitatory postsynaptic currents (mEPSCs) were manually
704 selected using Mini Analysis software (Synaptosoft), a standard program used for mEPSC event
705 detection and analysis. Records were filtered at 2 kHz using a low-pass Butterworth filter prior
706 to selection. The program threshold was set at 3 pA but the smallest mEPSC selected was 4.01

707 pA. MiniAnalysis selects many false positives with the automated feature when a small
708 threshold amplitude value is employed, due to random fluctuations in noise, so manual re-
709 evaluation of the automated process is necessary to eliminate false positives. If the threshold
710 value is set high, there are few false positives but small amplitude events that visually are
711 clearly mEPSCs are missed, and manual re-evaluation is necessary to add back false negatives or
712 the population ends up biased towards large mEPSC amplitudes. As soon as there is a manual
713 step, bias is introduced. Interestingly, a manual reevaluation step was applied in a recent study
714 that describes their process as 'unbiased' (Wu et al., 2020). In sum, we do not believe it is
715 currently possible to perform a completely unbiased detection process. A fully manual
716 detection process means that the same criterion ("does this *look* like an mEPSC?") is applied to
717 all events, not just the false positives, or the false negatives, which prevents the bias from being
718 primarily at one end or the other of the range of mEPSC amplitudes. It is important to note that
719 when performing the MiniAnalysis process, the researcher did not know whether a record was
720 from an untreated cell or a TTX-treated cell.
721 *Immunofluorescence, microscopy, and data analysis.* Primary cultures of mouse cortical
722 neurons were grown for 13-14 DIV. Antibodies to GluA2 (mouse ab against N-terminal, EMD
723 Millipore) were added directly to live cultures at 1:40 dilution, and incubated at 37 °C in a CO_2
724 incubator for 45 minutes. Cultures were rinsed 3 times with PBS/5% donkey serum before being
725 fixed with 4% paraformaldehyde. After 3 rinses in PBS/5% donkey serum, cultures were
726 incubated in CY3-labeled donkey-anti-mouse secondary antibodies for 1 hour at room
727 temperature, rinsed in PBS/5% donkey serum, permeabilized with 0.2% saponin, and incubated
728 in chick anti-MAP2 (1:2500, AbCAM) and rabbit anti-VGLUT1 (1:4000, Synaptic Systems) for 1

729 hour at room temperature in PBS/5% donkey serum. After rinsing with PBS/5% donkey serum,
730 coverslips were incubated with 488-anti chick and CY5-anti rabbit secondary antibodies for 1
731 hour at room temperature, rinsed, blotted to remove excess liquid, and inverted on a drop of
732 Vectashield (Vector Labs). Coverslips were sealed with nail polish and stored at 4 °C for < 1
733 week before imaging. All secondary antibodies were from Jackson Immunoresearch and were
734 used at 1:225 dilution.

735 Coverslips were viewed on a Fluoview FV1000 laser scanning confocal microscope with a
736 60x oil immersion, 1.35 NA objective. Once a pyramidal neuron was identified and a single
737 confocal section of the cell acquired (see Top, Figure 4), Fluoview 2.1 software was used to
738 zoom in on the primary dendrite (5X) and a series of confocal sections were taken every 0.5
739 μm. Images were analyzed offline with ImagePro 6 (Cybernetics). The composite image was
740 used to locate synaptic sites containing both VGLUT1 and GluA2 immunoreactivity in close
741 apposition to each other and to the primary dendrite or a secondary branch identified with
742 MAP2 immunoreactivity. An area of interest (AOI) was manually drawn around the GluA2
743 cluster in the confocal section in which it was the brightest. The AOIs for a dendrite were saved
744 in a single file; the AOI number and the confocal section it was associated with were noted for
745 later retrieval. For quantification, AOIs were loaded, an individual AOI was called up on the
746 appropriate section, and the count/measurement tool used to apply a threshold. Multiple
747 thresholds were used, 400-550, but we found that within a given experiment, the magnitude of
748 the TTX effect was not altered by different thresholds, therefore, all data presented here use a
749 threshold of 450. Pixels within the cluster that were above the threshold were automatically
750 outlined, and size, average intensity, and integral of the outlined region saved to Origin2020

751 (OriginLab) file for calculating mean values. For analyzing VGLUT1 sites, previous AOIs were
752 examined, and if not directly over the VGLUT1 site, moved to encompass it (this happened
753 when GluA2 and VGLUT1 were side by side rather than overlapping). The threshold was 200 for
754 all VGLUT1 data except Rab3A$^{+/+}$ Culture #1, where threshold was 400. There was no threshold
755 that worked for both that culture and the other cultures, with too much of the background
756 regions being included for Culture #1 with a threshold of 200, and too little of the synaptic site
757 area being included for the other Cultures with a threshold of 400.

758 *Statistics.* In our previous publication (Hanes et al., 2020), we described the characteristics of
759 homeostatic plasticity of mEPSC amplitudes in mouse cortical cultures using multiple mEPSC
760 amplitude quantiles from each cell to create data sets with thousands of samples. We
761 compared the cumulative distribution functions for mEPSC amplitudes in untreated vs. TTX-
762 treated cultures, as well as sorting the values from smallest to largest, and plotted TTX values
763 vs. control values in the rank order plot first described in (Turrigiano et al., 1998) to
764 demonstrate synaptic scaling. Finally, we plotted the ratio of TTX values/control values vs.
765 control values to show that the ratio, which represents the effect of TTX, increased with
766 increasing control values, which we termed "divergent scaling." Here, we wanted to avoid the
767 inflation of sample size caused by pooling multiple mEPSCs per cell in order to statistically
768 compare the effects of TTX in cultures of wild type mice, Rab3A$^{-/-}$ mice and Rab3A$^{Ebd/Ebd}$ mutant
769 mice. Therefore, we computed the mean mEPSC amplitude for each cell and compared means
770 from untreated and TTX-treated cultures with the non-parametric Kruskal-Wallis test, with N =
771 the number of cells. The overall means are presented ± SEM in the text, and p values are
772 displayed above each plot. The same process was carried out for the characteristics of synaptic

773 GluA2 receptor clusters and VGLUT1 sites in imaging experiments, with N = the number of
774 dendrites (one dendrite was sampled for each cell). Although we quantified three
775 characteristics of the GluA2 clusters and VGLUT1 sites, size, average intensity, and integral, we
776 have not corrected p values for multiple comparisons. Means are presented as box plots + data,
777 with the box at 25 and 75 percentiles, whiskers at 10 and 90 percentiles, a dot indicating the
778 mean, and a line indicating the median. In Figure 3, mEPSC amplitudes were measured within
779 the same cell before and after NASPM application, so a paired T test was used to compare the
780 pre- and post-NASPM mEPSC amplitudes. Statistics were computed and plots were created
781 using Origin2020 (OriginLab).
782
783
784 References
785

786 Araki Y, Lin DT, Huganir RL (2010) Plasma membrane insertion of the AMPA receptor GluA2 subunit is
787 regulated by NSF binding and Q/R editing of the ion pore. Proc Natl Acad Sci U S A 107:11080-
788 11085.
789 Benevento M, Iacono G, Selten M, Ba W, Oudakker A, Frega M, Keller J, Mancini R, Lewerissa E, Kleefstra
790 T, Stunnenberg HG, Zhou H, van Bokhoven H, Nadif Kasri N (2016) Histone Methylation by the
791 Kleefstra Syndrome Protein EHMT1 Mediates Homeostatic Synaptic Scaling. Neuron 91:341-355.
792 Benke T, Traynelis SF (2019) AMPA-Type Glutamate Receptor Conductance Changes and Plasticity: Still a
793 Lot of Noise. Neurochem Res 44:539-548.
794 Blaschke M, Keller BU, Rivosecchi R, Hollmann M, Heinemann S, Konnerth A (1993) A single amino acid
795 determines the subunit-specific spider toxin block of alpha-amino-3-hydroxy-5-methylisoxazole-
796 4-propionate/kainate receptor channels. Proc Natl Acad Sci U S A 90:6528-6532.
797 Bochet P, Audinat E, Lambolez B, Crepel F, Rossier J, Iino M, Tsuzuki K, Ozawa S (1994) Subunit
798 composition at the single-cell level explains functional properties of a glutamate-gated channel.
799 Neuron 12:383-388.
800 Burnashev N, Monyer H, Seeburg PH, Sakmann B (1992) Divalent ion permeability of AMPA receptor
801 channels is dominated by the edited form of a single subunit. Neuron 8:189-198.
802 Castillo PE, Janz R, Sudhof TC, Tzounopoulos T, Malenka RC, Nicoll RA (1997) Rab3A is essential for
803 mossy fibre long-term potentiation in the hippocampus. Nature 388:590-593.

804 Castren E, Zafra F, Thoenen H, Lindholm D (1992) Light regulates expression of brain-derived
805 neurotrophic factor mRNA in rat visual cortex. Proc Natl Acad Sci U S A 89:9444-9448.
806 Chang CW, Chiang CW, Jackson MB (2017) Fusion pores and their control of neurotransmitter and
807 hormone release. J Gen Physiol 149:301-322.
808 Cheresharov L, Ovtscharoff W, Manolov S (1978) Ultrastructural changes in the anterior horn synapses
809 of rat spinal cord under different locomotor conditions. J Neural Transm 42:9-21.
810 Chiang CW, Chang CW, Jackson MB (2018) The Transmembrane Domain of Synaptobrevin Influences
811 Neurotransmitter Flux through Synaptic Fusion Pores. J Neurosci 38:7179-7191.
812 Coleman WL, Bykhovskaia M (2009) Rab3a-mediated vesicle recruitment regulates short-term plasticity
813 at the mouse diaphragm synapse. Mol Cell Neurosci 41:286-296.
814 Coleman WL, Bykhovskaia M (2010) Cooperative regulation of neurotransmitter release by Rab3a and
815 synapsin II. Mol Cell Neurosci 44:190-200.
816 Coleman WL, Bill CA, Bykhovskaia M (2007) Rab3a deletion reduces vesicle docking and transmitter
817 release at the mouse diaphragm synapse. Neuroscience 148:1-6.
818 De Gois S, Schafer MK, Defamie N, Chen C, Ricci A, Weihe E, Varoqui H, Erickson JD (2005) Homeostatic
819 scaling of vesicular glutamate and GABA transporter expression in rat neocortical circuits. J
820 Neurosci 25:7121-7133.
821 Derkach V, Barria A, Soderling TR (1999) Ca2+/calmodulin-kinase II enhances channel conductance of
822 alpha-amino-3-hydroxy-5-methyl-4-isoxazolepropionate type glutamate receptors. Proc Natl
823 Acad Sci U S A 96:3269-3274.
824 Diaz-Rohrer B, Castello-Serrano I, Chan SH, Wang HY, Shurer CR, Levental KR, Levental I (2023) Rab3
825 mediates a pathway for endocytic sorting and plasma membrane recycling of ordered
826 microdomains. Proc Natl Acad Sci U S A 120:e2207461120.
827 Diering GH, Nirujogi RS, Roth RH, Worley PF, Pandey A, Huganir RL (2017) Homer1a drives homeostatic
828 scaling-down of excitatory synapses during sleep. Science 355:511-515.
829 Dubes S, Soula A, Benquet S, Tessier B, Poujol C, Favereaux A, Thoumine O, Letellier M (2022) miR-124-
830 dependent tagging of synapses by synaptopodin enables input-specific homeostatic plasticity.
831 EMBO J 41:e109012.
832 Fan D, Grooms SY, Araneda RC, Johnson AB, Dobrenis K, Kessler JA, Zukin RS (1999) AMPA receptor
833 protein expression and function in astrocytes cultured from hippocampus. J Neurosci Res
834 57:557-571.
835 Fernandes D, Carvalho AL (2016) Mechanisms of homeostatic plasticity in the excitatory synapse. J
836 Neurochem 139:973-996.
837 Fremeau RT, Jr., Kam K, Qureshi T, Johnson J, Copenhagen DR, Storm-Mathisen J, Chaudhry FA, Nicoll
838 RA, Edwards RH (2004) Vesicular glutamate transporters 1 and 2 target to functionally distinct
839 synaptic release sites. Science 304:1815-1819.
840 Geppert M, Bolshakov VY, Siegelbaum SA, Takei K, De Camilli P, Hammer RE, Sudhof TC (1994) The role
841 of Rab3A in neurotransmitter release. Nature 369:493-497.
842 Gu Y, Chiu SL, Liu B, Wu PH, Delannoy M, Lin DT, Wirtz D, Huganir RL (2016) Differential vesicular sorting
843 of AMPA and GABAA receptors. Proc Natl Acad Sci U S A 113:E922-931.
844 Hanes AL, Koesters AG, Fong MF, Altimimi HF, Stellwagen D, Wenner P, Engisch KL (2020) Divergent
845 Synaptic Scaling of Miniature EPSCs following Activity Blockade in Dissociated Neuronal Cultures.
846 J Neurosci 40:4090-4102.
847 Heir R, Abbasi Z, Komal P, Altimimi HF, Franquin M, Moschou D, Chambon J, Stellwagen D (2024)
848 Astrocytes Are the Source of TNF Mediating Homeostatic Synaptic Plasticity. J Neurosci 44.
849 Herlitze S, Raditsch M, Ruppersberg JP, Jahn W, Monyer H, Schoepfer R, Witzemann V (1993) Argiotoxin
850 detects molecular differences in AMPA receptor channels. Neuron 10:1131-1140.

851 Hollmann M, Hartley M, Heinemann S (1991) Ca2+ permeability of KA-AMPA--gated glutamate receptor
852 channels depends on subunit composition. Science 252:851-853.
853 Hong Y, Zhao T, Li XJ, Li S (2016) Mutant Huntingtin Impairs BDNF Release from Astrocytes by Disrupting
854 Conversion of Rab3a-GTP into Rab3a-GDP. J Neurosci 36:8790-8801.
855 Hou Q, Zhang D, Jarzylo L, Huganir RL, Man HY (2008) Homeostatic regulation of AMPA receptor
856 expression at single hippocampal synapses. Proc Natl Acad Sci U S A 105:775-780.
857 Hou Q, Ruan H, Gilbert J, Wang G, Ma Q, Yao WD, Man HY (2015) MicroRNA miR124 is required for the
858 expression of homeostatic synaptic plasticity. Nat Commun 6:10045.
859 Hu JH, Park JM, Park S, Xiao B, Dehoff MH, Kim S, Hayashi T, Schwarz MK, Huganir RL, Seeburg PH,
860 Linden DJ, Worley PF (2010) Homeostatic scaling requires group I mGluR activation mediated by
861 Homer1a. Neuron 68:1128-1142.
862 Hussain S, Davanger S (2015) Postsynaptic VAMP/Synaptobrevin Facilitates Differential Vesicle
863 Trafficking of GluA1 and GluA2 AMPA Receptor Subunits. PLoS One 10:e0140868.
864 Ibata K, Sun Q, Turrigiano GG (2008) Rapid synaptic scaling induced by changes in postsynaptic firing.
865 Neuron 57:819-826.
866 Iino M, Koike M, Isa T, Ozawa S (1996) Voltage-dependent blockage of Ca(2+)-permeable AMPA
867 receptors by joro spider toxin in cultured rat hippocampal neurones. J Physiol 496 (Pt 2):431-
868 437.
869 Jakawich SK, Neely RM, Djakovic SN, Patrick GN, Sutton MA (2010a) An essential postsynaptic role for
870 the ubiquitin proteasome system in slow homeostatic synaptic plasticity in cultured
871 hippocampal neurons. Neuroscience 171:1016-1031.
872 Jakawich SK, Nasser HB, Strong MJ, McCartney AJ, Perez AS, Rakesh N, Carruthers CJ, Sutton MA (2010b)
873 Local presynaptic activity gates homeostatic changes in presynaptic function driven by dendritic
874 BDNF synthesis. Neuron 68:1143-1158.
875 Jenkins MA, Traynelis SF (2012) PKC phosphorylates GluA1-Ser831 to enhance AMPA receptor
876 conductance. Channels (Austin) 6:60-64.
877 Jonas P, Burnashev N (1995) Molecular mechanisms controlling calcium entry through AMPA-type
878 glutamate receptor channels. Neuron 15:987-990.
879 Jurado S, Goswami D, Zhang Y, Molina AJ, Sudhof TC, Malenka RC (2013) LTP requires a unique
880 postsynaptic SNARE fusion machinery. Neuron 77:542-558.
881 Kapfhamer D, Valladares O, Sun Y, Nolan PM, Rux JJ, Arnold SE, Veasey SC, Bucan M (2002) Mutations in
882 Rab3a alter circadian period and homeostatic response to sleep loss in the mouse. Nat Genet
883 32:290-295.
884 Karunanithi S, Marin L, Wong K, Atwood HL (2002) Quantal size and variation determined by vesicle size
885 in normal and mutant Drosophila glutamatergic synapses. J Neurosci 22:10267-10276.
886 Kavalali ET, Monteggia LM (2023) Rapid homeostatic plasticity and neuropsychiatric therapeutics.
887 Neuropsychopharmacology 48:54-60.
888 Kawana E, Akert K, Bruppacher H (1971) Enlargement of synaptic vesicles as an early sign of terminal
889 degneration in the rat caudate nucleus. J Comp Neurol 142:297-307.
890 Kennedy MJ, Davison IG, Robinson CG, Ehlers MD (2010) Syntaxin-4 defines a domain for activity-
891 dependent exocytosis in dendritic spines. Cell 141:524-535.
892 Koike M, Iino M, Ozawa S (1997) Blocking effect of 1-naphthyl acetyl spermine on Ca(2+)-permeable
893 AMPA receptors in cultured rat hippocampal neurons. Neurosci Res 29:27-36.
894 Kristensen AS, Jenkins MA, Banke TG, Schousboe A, Makino Y, Johnson RC, Huganir R, Traynelis SF
895 (2011) Mechanism of Ca2+/calmodulin-dependent kinase II regulation of AMPA receptor gating.
896 Nat Neurosci 14:727-735.
897 Leenders AG, Lopes da Silva FH, Ghijsen WE, Verhage M (2001) Rab3a is involved in transport of synaptic
898 vesicles to the active zone in mouse brain nerve terminals. Mol Biol Cell 12:3095-3102.

899 Lignani G, Baldelli P, Marra V (2020) Homeostatic Plasticity in Epilepsy. Front Cell Neurosci 14:197.
900 Lledo PM, Zhang X, Sudhof TC, Malenka RC, Nicoll RA (1998) Postsynaptic membrane fusion and long-
901 term potentiation. Science 279:399-403.
902 Lloret IL, Saavedra JP (1975) Enlargement of synaptic vesicles in degenerating nerve endings: a
903 comparison between cat and monkey. J Neurocytol 4:1-6.
904 Lonart G, Janz R, Johnson KM, Sudhof TC (1998) Mechanism of action of rab3A in mossy fiber LTP.
905 Neuron 21:1141-1150.
906 Lovinger DM, Abrahao KP (2018) Synaptic plasticity mechanisms common to learning and alcohol use
907 disorder. Learn Mem 25:425-434.
908 Maienschein V, Marxen M, Volknandt W, Zimmermann H (1999) A plethora of presynaptic proteins
909 associated with ATP-storing organelles in cultured astrocytes. Glia 26:233-244.
910 Miyasaka Y, Yamamoto N (2021) Neuronal Activity Patterns Regulate Brain-Derived Neurotrophic Factor
911 Expression in Cortical Cells via Neuronal Circuits. Front Neurosci 15:699583.
912 Nishimune A, Isaac JT, Molnar E, Noel J, Nash SR, Tagaya M, Collingridge GL, Nakanishi S, Henley JM
913 (1998) NSF binding to GluR2 regulates synaptic transmission. Neuron 21:87-97.
914 O'Brien RJ, Kamboj S, Ehlers MD, Rosen KR, Fischbach GD, Huganir RL (1998) Activity-dependent
915 modulation of synaptic AMPA receptor accumulation. Neuron 21:1067-1078.
916 Oh MC, Derkach VA (2005) Dominant role of the GluR2 subunit in regulation of AMPA receptors by
917 CaMKII. Nat Neurosci 8:853-854.
918 Ormel L, Stensrud MJ, Bergersen LH, Gundersen V (2012) VGLUT1 is localized in astrocytic processes in
919 several brain regions. Glia 60:229-238.
920 Osten P, Srivastava S, Inman GJ, Vilim FS, Khatri L, Lee LM, States BA, Einheber S, Milner TA, Hanson PI,
921 Ziff EB (1998) The AMPA receptor GluR2 C terminus can mediate a reversible, ATP-dependent
922 interaction with NSF and alpha- and beta-SNAPs. Neuron 21:99-110.
923 Pozo K, Goda Y (2010) Unraveling mechanisms of homeostatic synaptic plasticity. Neuron 66:337-351.
924 Riedel D, Antonin W, Fernandez-Chacon R, Alvarez de Toledo G, Jo T, Geppert M, Valentijn JA, Valentijn
925 K, Jamieson JD, Sudhof TC, Jahn R (2002) Rab3D is not required for exocrine exocytosis but for
926 maintenance of normally sized secretory granules. Mol Cell Biol 22:6487-6497.
927 Rutherford LC, Nelson SB, Turrigiano GG (1998) BDNF has opposite effects on the quantal amplitude of
928 pyramidal neuron and interneuron excitatory synapses. Neuron 21:521-530.
929 Sanderson JL, Scott JD, Dell'Acqua ML (2018) Control of Homeostatic Synaptic Plasticity by AKAP-
930 Anchored Kinase and Phosphatase Regulation of Ca(2+)-Permeable AMPA Receptors. J Neurosci
931 38:2863-2876.
932 Schluter OM, Basu J, Sudhof TC, Rosenmund C (2006) Rab3 superprimes synaptic vesicles for release:
933 implications for short-term synaptic plasticity. J Neurosci 26:1239-1246.
934 Schonn JS, van Weering JR, Mohrmann R, Schluter OM, Sudhof TC, de Wit H, Verhage M, Sorensen JB
935 (2010) Rab3 proteins involved in vesicle biogenesis and priming in embryonic mouse chromaffin
936 cells. Traffic 11:1415-1428.
937 Shepherd JD, Rumbaugh G, Wu J, Chowdhury S, Plath N, Kuhl D, Huganir RL, Worley PF (2006)
938 Arc/Arg3.1 mediates homeostatic synaptic scaling of AMPA receptors. Neuron 52:475-484.
939 Silva MM, Rodrigues B, Fernandes J, Santos SD, Carreto L, Santos MAS, Pinheiro P, Carvalho AL (2019)
940 MicroRNA-186-5p controls GluA2 surface expression and synaptic scaling in hippocampal
941 neurons. Proc Natl Acad Sci U S A 116:5727-5736.
942 Smith-Dijak AI, Nassrallah WB, Zhang LYJ, Geva M, Hayden MR, Raymond LA (2019) Impairment and
943 Restoration of Homeostatic Plasticity in Cultured Cortical Neurons From a Mouse Model of
944 Huntington Disease. Front Cell Neurosci 13:209.
945 Soares C, Lee KF, Nassrallah W, Beique JC (2013) Differential subcellular targeting of glutamate receptor
946 subtypes during homeostatic synaptic plasticity. J Neurosci 33:13547-13559.

947 Soden ME, Chen L (2010) Fragile X protein FMRP is required for homeostatic plasticity and regulation of
948 synaptic strength by retinoic acid. J Neurosci 30:16910-16921.
949 Song I, Kamboj S, Xia J, Dong H, Liao D, Huganir RL (1998) Interaction of the N-ethylmaleimide-sensitive
950 factor with AMPA receptors. Neuron 21:393-400.
951 Stellwagen D, Malenka RC (2006) Synaptic scaling mediated by glial TNF-alpha. Nature 440:1054-1059.
952 Stellwagen D, Beattie EC, Seo JY, Malenka RC (2005) Differential regulation of AMPA receptor and GABA
953 receptor trafficking by tumor necrosis factor-alpha. J Neurosci 25:3219-3228.
954 Suh YH, Terashima A, Petralia RS, Wenthold RJ, Isaac JT, Roche KW, Roche PA (2010) A neuronal role for
955 SNAP-23 in postsynaptic glutamate receptor trafficking. Nat Neurosci 13:338-343.
956 Sun HY, Bartley AF, Dobrunz LE (2009) Calcium-permeable presynaptic kainate receptors involved in
957 excitatory short-term facilitation onto somatostatin interneurons during natural stimulus
958 patterns. J Neurophysiol 101:1043-1055.
959 Sutton MA, Ito HT, Cressy P, Kempf C, Woo JC, Schuman EM (2006) Miniature neurotransmission
960 stabilizes synaptic function via tonic suppression of local dendritic protein synthesis. Cell
961 125:785-799.
962 Suzuki K, Kim JW, Nosyreva E, Kavalali ET, Monteggia LM (2021) Convergence of distinct signaling
963 pathways on synaptic scaling to trigger rapid antidepressant action. Cell Rep 37:109918.
964 Tatavarty V, Sun Q, Turrigiano GG (2013) How to scale down postsynaptic strength. J Neurosci 33:13179-
965 13189.
966 Thapliyal S, Arendt KL, Lau AG, Chen L (2022) Retinoic acid-gated BDNF synthesis in neuronal dendrites
967 drives presynaptic homeostatic plasticity. Elife 11.
968 Tian M, Xu CS, Montpetit R, Kramer RH (2012) Rab3A mediates vesicle delivery at photoreceptor ribbon
969 synapses. J Neurosci 32:6931-6936.
970 Tononi G, Cirelli C (2014) Sleep and the price of plasticity: from synaptic and cellular homeostasis to
971 memory consolidation and integration. Neuron 81:12-34.
972 Torrado Pacheco A, Bottorff J, Gao Y, Turrigiano GG (2021) Sleep Promotes Downward Firing Rate
973 Homeostasis. Neuron 109:530-544 e536.
974 Trasande CA, Ramirez JM (2007) Activity deprivation leads to seizures in hippocampal slice cultures: is
975 epilepsy the consequence of homeostatic plasticity? J Clin Neurophysiol 24:154-164.
976 Turrigiano GG, Nelson SB (2004) Homeostatic plasticity in the developing nervous system. Nat Rev
977 Neurosci 5:97-107.
978 Turrigiano GG, Leslie KR, Desai NS, Rutherford LC, Nelson SB (1998) Activity-dependent scaling of
979 quantal amplitude in neocortical neurons. Nature 391:892-896.
980 Wang JKT, Langfelder P, Horvath S, Palazzolo MJ (2017) Exosomes and Homeostatic Synaptic Plasticity
981 Are Linked to Each other and to Huntington's, Parkinson's, and Other Neurodegenerative
982 Diseases by Database-Enabled Analyses of Comprehensively Curated Datasets. Front Neurosci
983 11:149.
984 Wang X, Thiagarajan R, Wang Q, Tewolde T, Rich MM, Engisch KL (2008) Regulation of quantal shape by
985 Rab3A: evidence for a fusion pore-dependent mechanism. J Physiol 586:3949-3962.
986 Wang X, Wang Q, Yang S, Bucan M, Rich MM, Engisch KL (2011) Impaired activity-dependent plasticity of
987 quantal amplitude at the neuromuscular junction of Rab3A deletion and Rab3A earlybird mutant
988 mice. J Neurosci 31:3580-3588.
989 Wang X, Li Y, Engisch KL, Nakanishi ST, Dodson SE, Miller GW, Cope TC, Pinter MJ, Rich MM (2005)
990 Activity-dependent presynaptic regulation of quantal size at the mammalian neuromuscular
991 junction in vivo. J Neurosci 25:343-351.
992 Watt AJ, van Rossum MC, MacLeod KM, Nelson SB, Turrigiano GG (2000) Activity coregulates quantal
993 AMPA and NMDA currents at neocortical synapses. Neuron 26:659-670.

994 Weisskopf MG, Castillo PE, Zalutsky RA, Nicoll RA (1994) Mediation of hippocampal mossy fiber long-
995 term potentiation by cyclic AMP. Science 265:1878-1882.
996 Wierenga CJ, Ibata K, Turrigiano GG (2005) Postsynaptic expression of homeostatic plasticity at
997 neocortical synapses. J Neurosci 25:2895-2905.
998 Wilson NR, Kang J, Hueske EV, Leung T, Varoqui H, Murnick JG, Erickson JD, Liu G (2005) Presynaptic
999 regulation of quantal size by the vesicular glutamate transporter VGLUT1. J Neurosci 25:6221-
1000 6234.
1001 Wu D, Bacaj T, Morishita W, Goswami D, Arendt KL, Xu W, Chen L, Malenka RC, Sudhof TC (2017)
1002 Postsynaptic synaptotagmins mediate AMPA receptor exocytosis during LTP. Nature 544:316-
1003 321.
1004 Wu YK, Hengen KB, Turrigiano GG, Gjorgjieva J (2020) Homeostatic mechanisms regulate distinct aspects
1005 of cortical circuit dynamics. Proc Natl Acad Sci U S A 117:24514-24525.
1006 Xu X, Pozzo-Miller L (2017) EEA1 restores homeostatic synaptic plasticity in hippocampal neurons from
1007 Rett syndrome mice. J Physiol 595:5699-5712.

1008

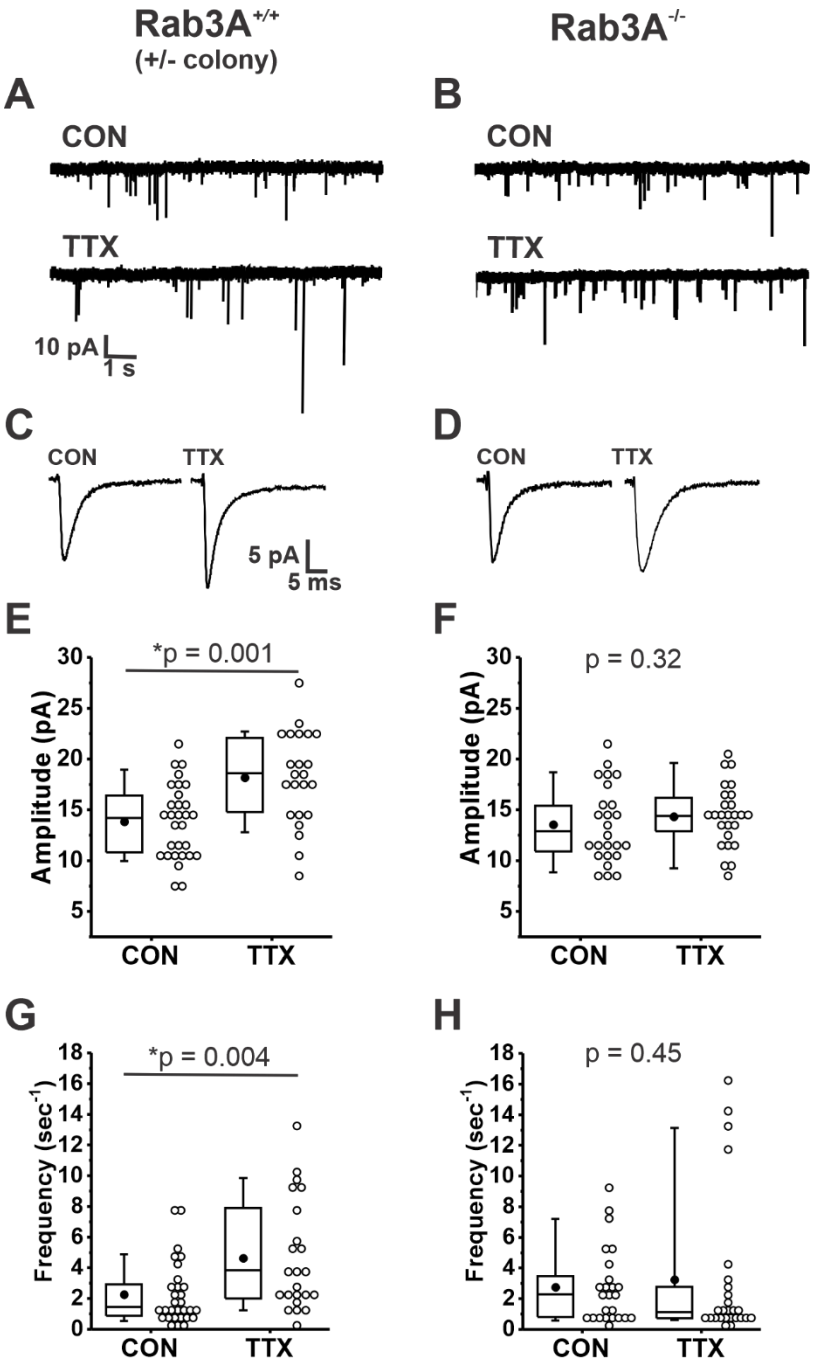

Figure 1. Loss of Rab3A prevented the TTX-induced increases in amplitudes and frequency of mEPSCs recorded in cultured mouse cortical neurons.

(A) Ten second example traces recorded at -60 mV in pyramidal cortical neurons from an untreated ("CON") and TTX-treated ("TTX") neuron in cultures prepared from Rab3A$^{+/+}$ mice from the Rab3A$^{+/-}$ colony. (B) Ten second example traces recorded at -60 mV in pyramidal cortical neurons from an untreated ("CON") and TTX-treated ("TTX") neuron in cultures prepared from Rab3A$^{-/-}$ mice. (C & D) Average traces for the recordings shown in A and B,

respectively. (E) Box plots for average mEPSC amplitudes from untreated cells and TTX-treated cells in cultures prepared from Rab3A$^{+/+}$ mice (Rab3A$^{+/-}$ colony; CON, N = 30 cells, 13.9 ± 0.7 pA; TTX, N = 23 cells, 18.2 ± 0.9 pA; from 11 cultures). (F) Box plots for average mEPSC amplitudes from untreated cells and TTX-treated cells in cultures prepared from Rab3A$^{-/-}$ mice (CON, N = 25 cells, 13.6 ± 0.7 pA; TTX, N = 26 cells, 14.3 ± 0.6 pA); from 11 cultures. (G) Box plots for average mEPSC frequency for same Rab3A$^{+/+}$ cells as in (E) (CON, 2.26 ± 0.37 sec^{-1}; TTX, 4.62 ± 0.74 sec^{-1}). (H) Box plots for average mEPSC frequency for same Rab3A$^{-/-}$cells as in (F) (CON, 2.74 ± 0.49 sec^{-1}; TTX, 3.23 ± 0.93 sec^{-1}). Box plot parameters: box ends, 25th and 75th percentiles; whiskers, 10th and 90th percentiles; open circles represent means from individual cells; line, median; dot, mean. p values (shown on the graphs) are from Kruskal-Wallis test. For all p-values, * with underline indicates significance with $p < 0.05$.

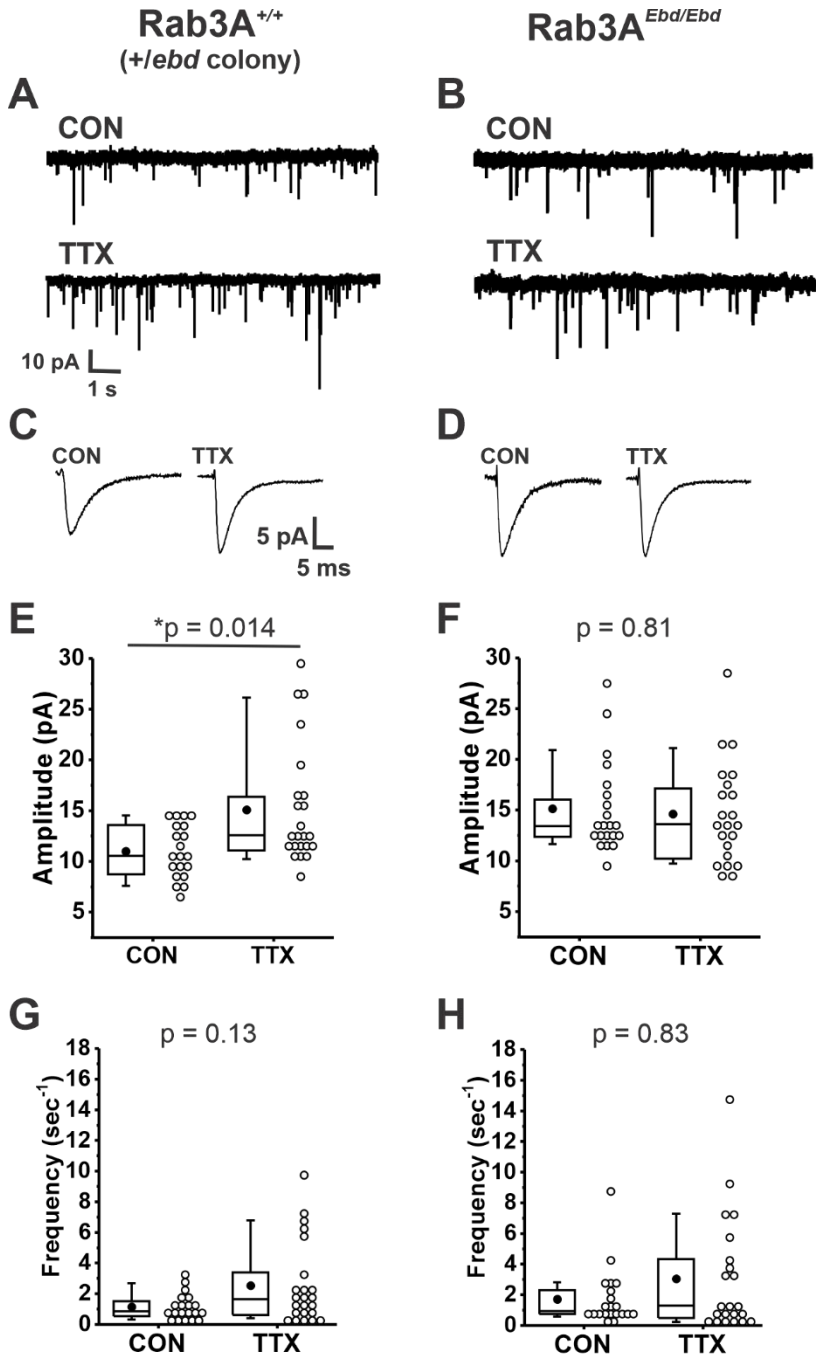

Figure 2. Normally functioning Rab3A was required for TTX-induced homeostatic plasticity of mEPSC amplitudes in cultured mouse cortical neurons.

(A) Ten second example traces recorded at -60 mV in pyramidal cortical neurons from an untreated ("CON") and TTX-treated ("TTX") neuron in cultures prepared from Rab3A$^{+/+}$ mice from the Rab3A$^{+/Ebd}$ colony. (B) Ten second example traces recorded at -60 mV in pyramidal cortical neurons from an untreated ("CON") and TTX-treated ("TTX") neuron in cultures

prepared from Rab3A$^{Ebd/Ebd}$ mice. (C & D) Average traces for the recordings shown in A and B, respectively. (E) Box plots for average mEPSC amplitudes from untreated cells and TTX-treated cells from cultures prepared from Rab3A$^{+/+}$ mice (Rab3A$^{+/Ebd}$ colony; CON, N = 20 cells, 11.0 ± 0.6 pA; TTX, N = 23 cells, 15.1 ± 1.2 pA; from 6 cultures). (F) Box plots for average mEPSC amplitudes from untreated cells and TTX-treated cells from cultures prepared from Rab3A$^{Ebd/Ebd}$ mice (CON, N = 21 cells, 15.1 ± 1.0 pA; TTX, N = 22 cells, 14.6 ± 1.1 pA; from 7 cultures.) (G) Box plots for average mEPSC frequency for same Rab3A$^{+/+}$ cells as in (E) (CON, 1.15 ± 0.19 sec^{-1}; TTX, 2.54 ± 0.55 sec^{-1}). (H) Box plots for average mEPSC frequency for same Rab3A$^{Ebd/Ebd}$ cells as in (F) (CON, 1.71 ± 0.41 sec^{-1}; TTX, 3.05 ± 0.80 sec^{-1}). Box plot parameters: box ends, 25th and 75th percentiles; whiskers, 10th and 90th percentiles; open circles represent means from individual cells; line, median; dot, mean. p values (shown on the graphs) are from Kruskal-Wallis test. For all p-values, * with underline indicates significance with $p < 0.05$.

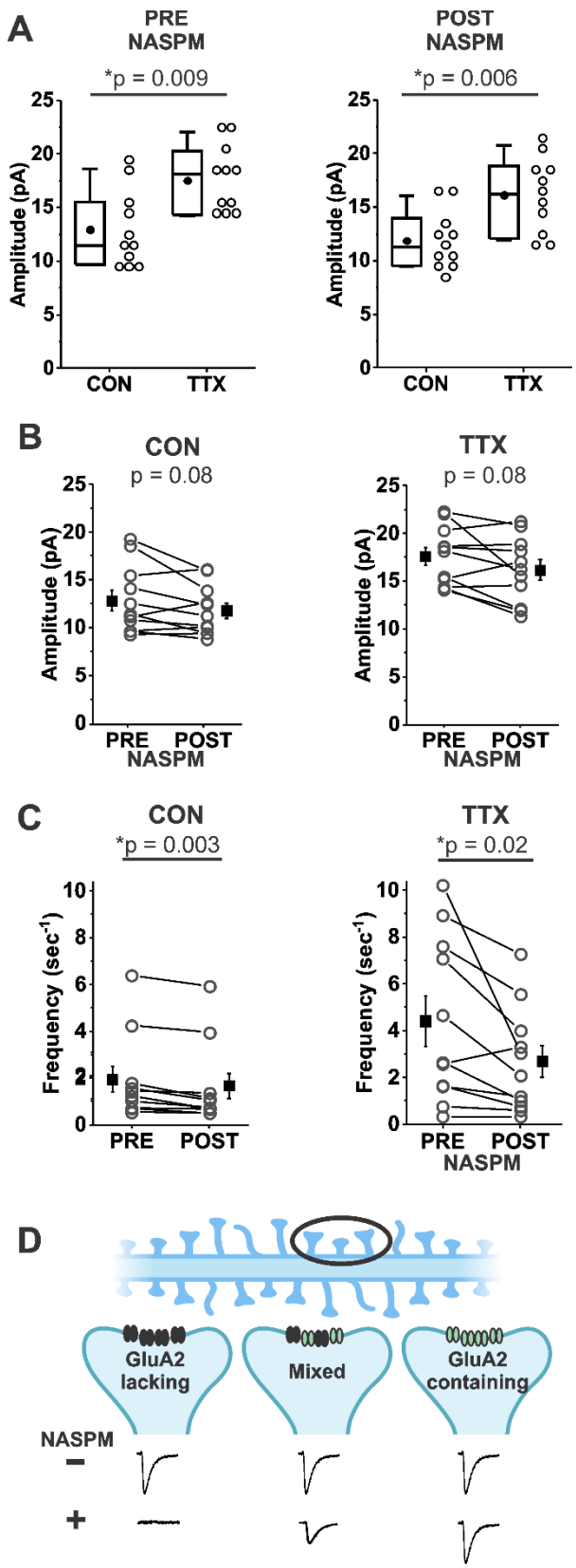
A
PRE NASPM
*p = 0.009
POST NASPM
*p = 0.006
Amplitude (pA)
CON
TTX
B
CON
p = 0.08
TTX
p = 0.08
Amplitude (pA)
PRE
POST
NASPM
C
CON
*p = 0.003
TTX
*p = 0.02
Frequency (sec-1)
PRE
POST
NASPM
D
GluA2 lacking
Mixed
GluA2 containing
NASPM
−
+

Figure 3

Figure 3. Homeostatic plasticity of mEPSC amplitudes in mouse cortical cultures treated with TTX for 48 hr was not affected by acute inhibition of Ca^{2+} permeable AMPA receptors by NASPM (20 μm).

(A) Box plot comparison of the TTX effect on mEPSC amplitudes in the same pyramidal neurons before and after application of 20 μM NASPM. (N = 11 cells from 3 cultures; Pre-NASPM, CON: 12.9 ± 1.1 pA; TTX: 17.5 ± 0.9 pA; post-NASPM, CON: 11.9 ± 0.8 pA; TTX: 16.1 ± 1.0 pA). (B) Line series plot of mEPSC amplitudes before and after acute perfusion with 20 μM NASPM for untreated and TTX-treated pyramidal neurons; same cells as in (A); CON, pre-NASPM: 12.9 ± 1.1 pA; post-NASPM: 11.9 ± 0.8 pA; TTX, pre-NASPM: 17.5 ± 0.9 pA; post-NASPM: 16.1 ± 0.1 pA. (C) Line series plot of mEPSC frequency before and after acute perfusion with 20 μM NASPM for untreated and TTX-treated pyramidal neurons; same cells as in (A); CON, pre-NAPSM: 1.84 ± 0.55 sec^{-1}; post-NASPM; 1.56 ± 0.53 sec^{-1}; TTX, pre-NASPM: 4.40 ± 1.06 sec^{-1}; post-NASPM, 2.68 ± 0.68 sec^{-1}. (D) A proposed mechanism for why NASPM had a robust effect on frequency without greatly affecting amplitude. A dendrite with spines (Top) is expanded on three postsynaptic sites (Middle) to show possible types of AMPA receptor distributions: Left, at a site comprised only of Ca^{2+}-permeable AMPA receptors (NASPM-sensitive, GluA2-lacking receptors (black)), NASPM would completely inhibit the mEPSC, causing a decrease in frequency to be measured in the overall population; Right, at a site comprised only of Ca^{2+}-impermeable AMPA receptors (NASPM-insensitive, GluA2-containing receptors (green)), NASPM would have no effect on mEPSC amplitude; Middle, at a site comprised of a mix of Ca^{2+}-permeable and Ca^{2+}-impermeable AMPA receptors, NASPM would partially inhibit the mEPSC. Diagram produced in BioRender.com (2024). Box plot parameters: box ends, 25th and 75th percentiles; whiskers, 10th and 90th percentiles; open circles represent means from individual cells; line, median; dot, mean. p values (shown on the graphs) are from Kruskal-Wallis test. Line series plot p values are from student's paired t test. For all p-values, * with underline indicates significance with $p < 0.05$.

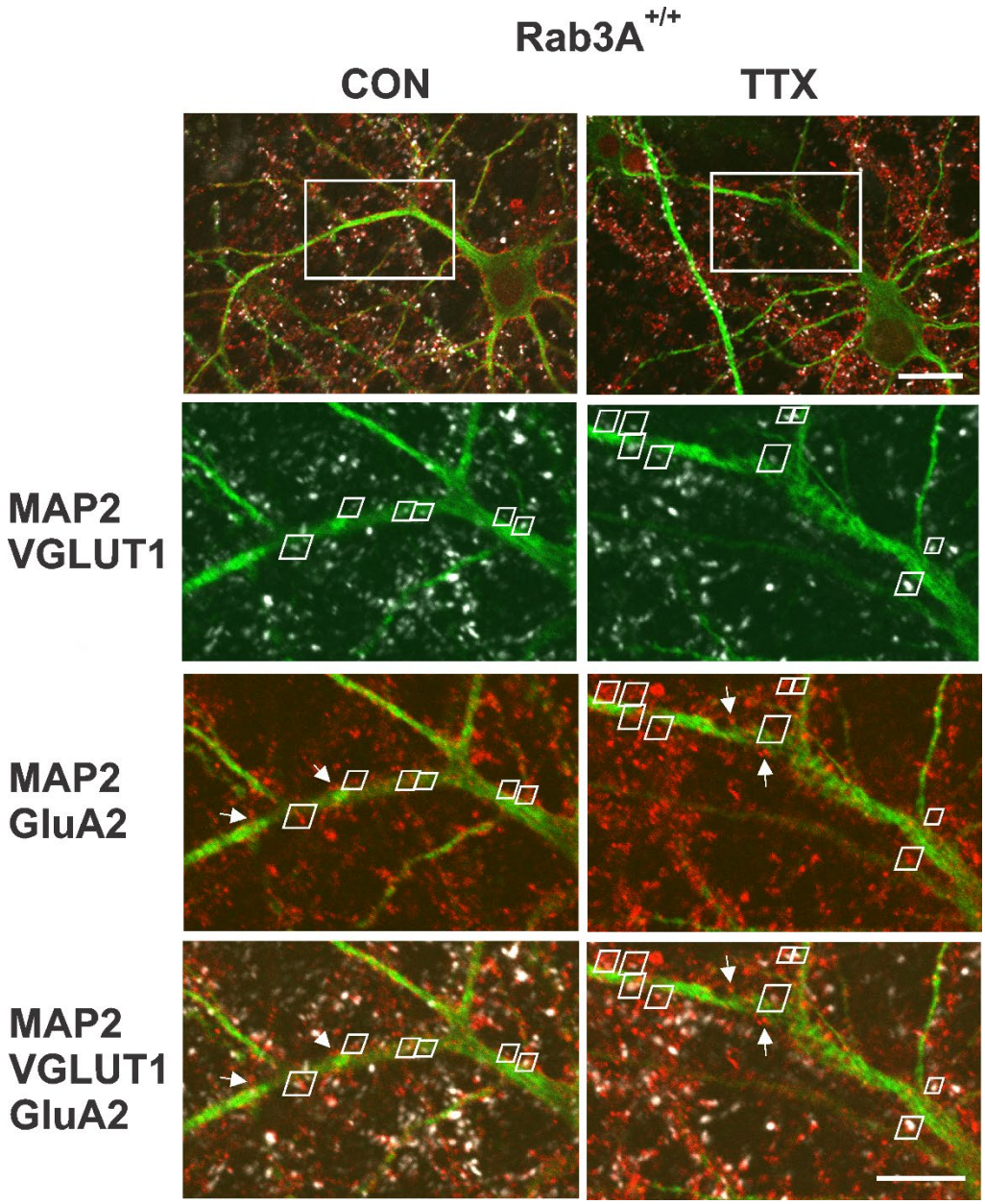

Figure 4. Identification of synaptic GluA2 receptor immunofluorescence on primary dendrites of pyramidal neurons in high density mouse cortical co-cultures prepared from Rab3A$^{+/+}$ mice.

(Top) Non-zoomed single confocal sections collected with a 60X oil immersion objective of recognizably pyramidal-shaped neurons, presumed to be excitatory neurons, selected for synaptic GluA2 analysis. A neuron was selected from an untreated coverslip (CON, Left) and a TTX-treated coverslip (TTX, Right) from the same culture prepared from Rab3A$^{+/+}$ animals (= Rab3A$^{+/+}$ Culture #2 in Figure 6). The white rectangular boxes indicate 5X zoomed areas shown in the images below. Note that the depth of the single confocal section of the non-zoomed neuron image is not at the same depth as the confocal section in zoomed dendritic image, so

some features are not visible in both images. Scale bar, 20 μm. (Bottom) 5X zoom single confocal sections selected for demonstration purposes because they had an unusually high number of identified synaptic pairs along the primary dendrite contained within a single confocal section. Synaptic pairs, highlighted with white trapezoids, were identified based on close proximity of GluA2 (red) and VGLUT1 (white) immunofluorescence, apposed to the MAP2 immunofluorescent primary dendrite (green). Some apparent synaptic pairs are not highlighted with a white trapezoid because there was a different confocal section in which the two immunofluorescent sites were maximally bright. There were GluA2 positive clusters located on the primary dendrites that were not apposed to VGLUT1-positive terminals (4 of these non-synaptic GluA2 clusters are highlighted with white arrows in the MAP2-GluA2 and MAP2-GluA2-VGLUT1 panels). Scale bar, 10 μm.

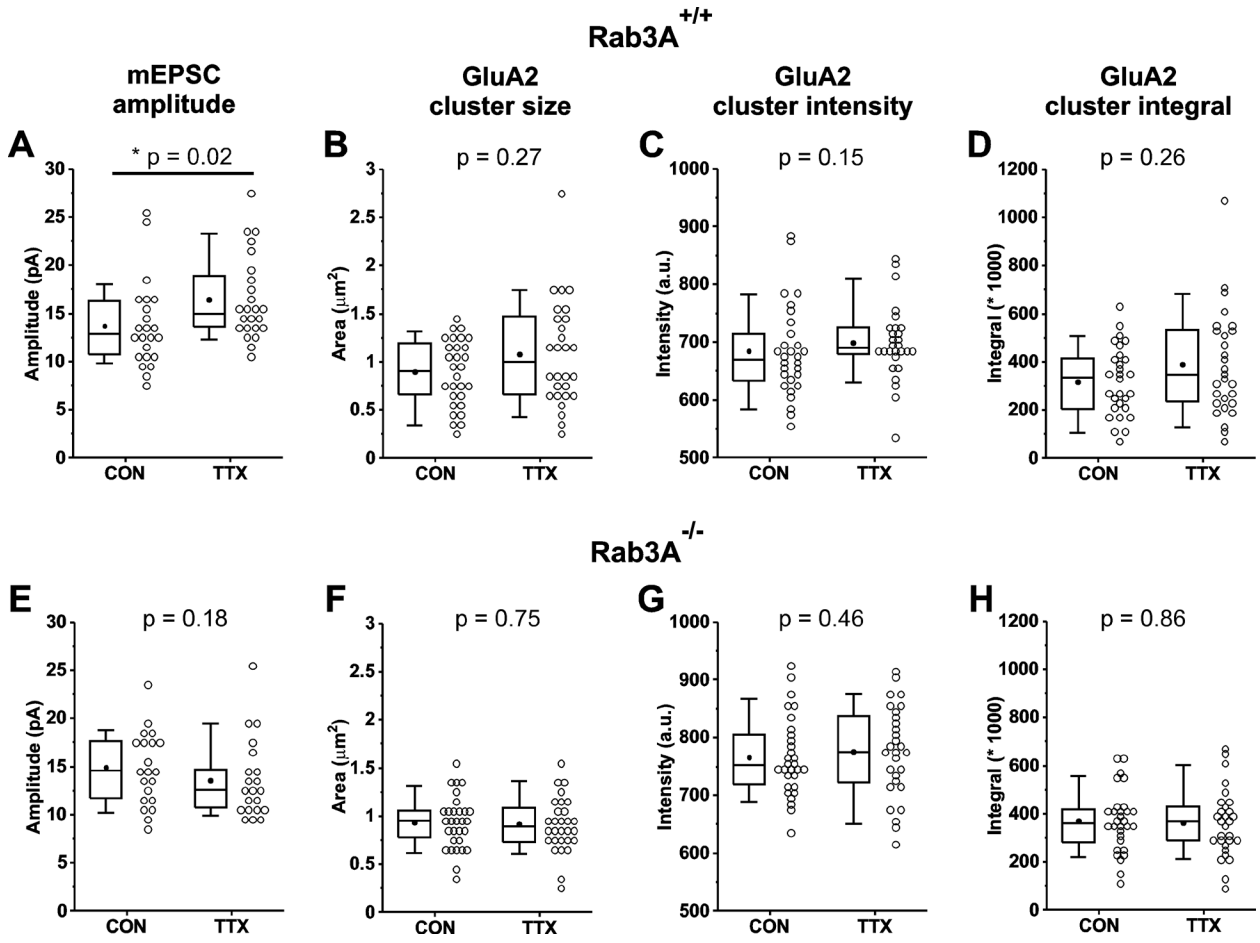

Figure 5. Comparison of mEPSC amplitude and GluA2 receptor cluster data, pooled from 3 cortical co-cultures prepared from Rab3A$^{+/+}$ mice and 3 co-cultures prepared from Rab3A$^{-/-}$ mice.

(A) Mean mEPSC amplitudes recorded in pyramidal neurons from untreated (CON) and TTX-treated coverslips (TTX) of co-cultures prepared from Rab3A$^{+/+}$ mice (CON, N = 23 cells, 13.7 $\pm$ 0.9 pA; TTX, N = 24 cells, 16.4 $\pm$ 0.9 pA; from 3 cultures). (B) Mean sizes of synaptic GluA2 receptor clusters, identified by proximity to VGLUT1-positive terminals, on primary dendrites of pyramidal neurons of untreated and TTX-treated coverslips from the same cultures as in (A) (CON, N = 29 dendrites, 0.90 $\pm$ 0.06 μm^2; TTX, N = 28 dendrites, 1.08 $\pm$ 0.10 μm^2). (C) Mean intensities of the same GluA2 receptor clusters as in (B) (CON, 684 $\pm$ 15 A.U.; TTX, 699 $\pm$ 12 A.U.). (D) Mean integrals of the same GluA2 receptor clusters as in (B). (CON, 317,898 $\pm$ 26,726 A.U.; TTX, 389,487 $\pm$ 41,465 A.U.). (E) Mean mEPSC amplitudes in pyramidal neurons from untreated and TTX-treated coverslips of mouse cortical co-cultures from Rab3A$^{-/-}$ mice (CON, N = 21 cells, 14.9 $\pm$ 0.8 pA; TTX, N = 21 cells, 13.5 $\pm$ 0.9 pA; from 3 cultures). (F) Mean sizes of GluA2 receptor clusters, identified by proximity to VGLUT1-positive terminals, on primary dendrites of pyramidal neurons of untreated and TTX-treated coverslips from the same cultures

as in (E). (CON, N = 30 dendrites, 0.93 $\pm$ 0.05 μm^2; TTX, N = 30 dendrites, 0.92 $\pm$ 0.05 μm^2). (G) Mean intensities of the same GluA2 receptor clusters as in (F). (CON, 766 $\pm$ 12 A.U.; TTX, 776 $\pm$ 78 A.U.). (H) Mean integrals of the same GluA2 receptor clusters as in (F). (CON, 369,436 $\pm$ 23,439 A.U.; TTX, 366,389 $\pm$ 25,049 A.U.). Box plot parameters: box ends, 25th and 75th percentiles; whiskers, 10 and 90 percentiles; open circles indicate means of individual cells; line, median; dot, mean. p values (shown on the graphs) were determined with Kruskal-Wallis test. For all p-values, * with underline indicates significance with $p < 0.05$.

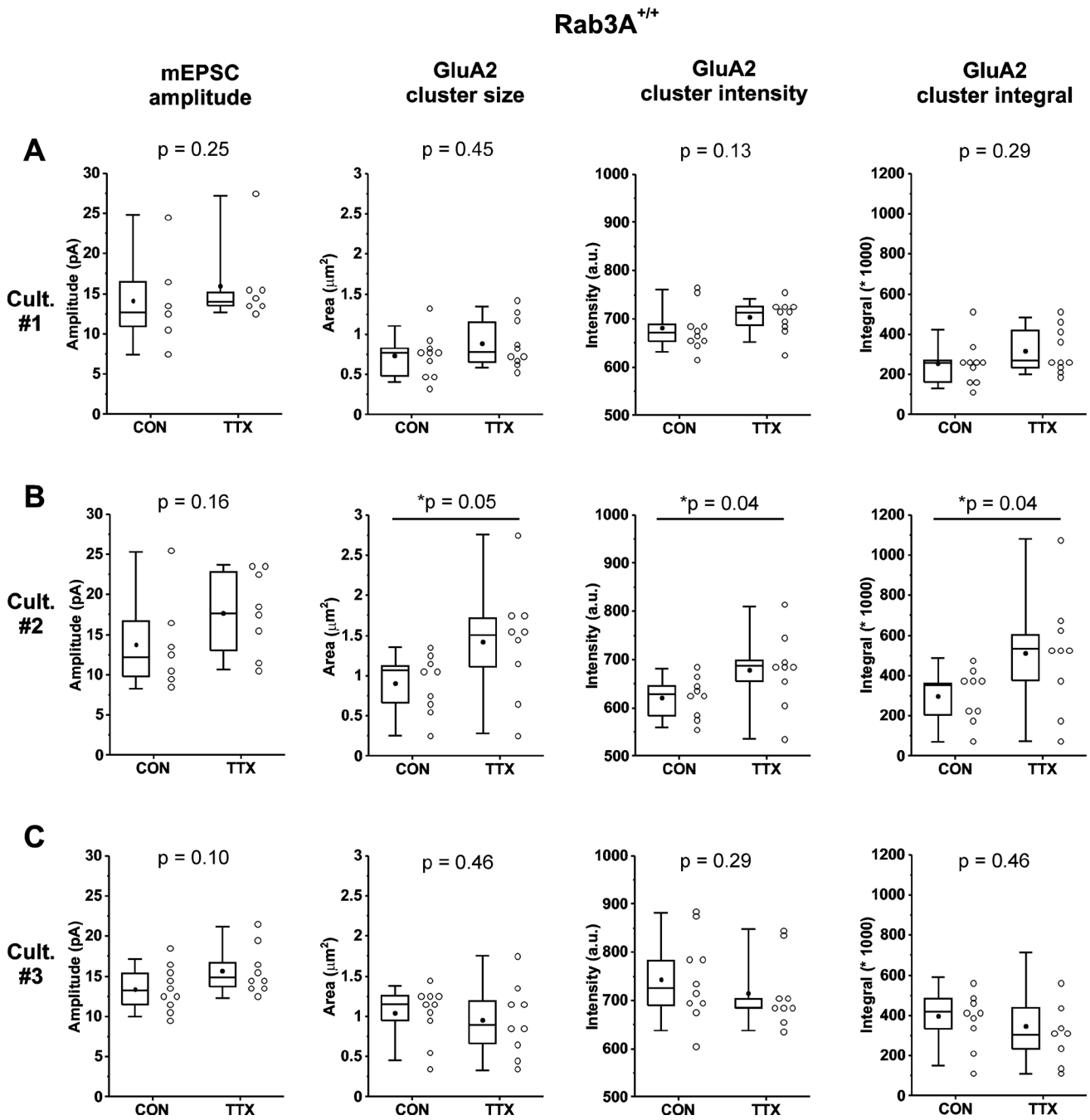

Figure 6. In cultures prepared from Rab3A$^{+/+}$ mice, increases in mEPSC amplitudes following TTX treatment were not always matched by increases in GluA2 receptor cluster characteristics.

(A) Culture #1: mean mEPSC amplitudes for pyramidal neurons from untreated coverslips (CON) and TTX-treated coverslips (TTX) (CON, N = 6, 14.2 $\pm$ 2.2 pA; TTX, N = 6, 15.9 $\pm$ 1.9 pA), compared to mean sizes, intensities, and integrals of synaptic GluA2 receptor clusters in images taken of dendrites from other coverslips in the same culture (CON, N = 10, TTX, N = 9; size, CON, 0.73 $\pm$ 0.09 μm^2; TTX, 0.89 $\pm$ 0.09 μm^2; intensity, CON, 682 $\pm$ 15 A.U.; TTX, 704 $\pm$ 11 A.U.;

integral, CON, 256,364 ± 35,242 A.U.; TTX, 316,647 ± 35,077 A.U.). (B) Culture #2: mean mEPSC amplitudes for pyramidal neurons from untreated and TTX-treated coverslips (CON, N = 7, 13.8 ± 2.4 pA; TTX, N = 8, 17.7 ± 1.8 pA), compared to mean sizes, intensities, and integrals of synaptic GluA2 receptor clusters in images taken of dendrites from other coverslips from the same culture (CON, N = 9, TTX, N = 9; size, CON, 0.91 ± 0.12 μm^2; TTX, 1.42 ± 0.24 μm^2; intensity, CON, 621 ± 14 A.U.; TTX, 679 ± 26 A.U.; integral, CON, 296,300 ± 44,108 A.U.; TTX, 512,336 ± 96,892 A.U.). (C) Culture #3: mean mEPSC amplitudes for pyramidal neurons from untreated coverslips and TTX-treated coverslips (CON, N = 10, 13.4 ± 0.8 pA; TTX, N = 9, 15.7 ± 1.0 pA,) compared to mean sizes, intensities, and integrals of synaptic GluA2 receptor clusters in images taken from other coverslips from the same culture. (CON, N = 10, TTX, N = 9; size, CON, 1.05 ± 0.11 μm^2; TTX, 0.95 ± 0.15 μm^2; intensity, CON, 744 ± 28 A.U.; TTX, 714 ± 25 A.U.; integral, CON, 398,870 ± 49,500 A.U.; TTX, 347,571 ± 65,454 A.U.). Cultures were fixed and processed for immunofluorescence on the same day as mEPSC recordings, and imaged within 1 week. Box plot parameters: box ends, 25th and 75th percentiles; whiskers, 10th and 90th percentiles; open circles represent means from individual cells; line, median; dot, mean. p values (shown on the graphs) are from Kruskal-Wallis test. p-values denoted with * and underline indicates significance of $p < 0.05$.

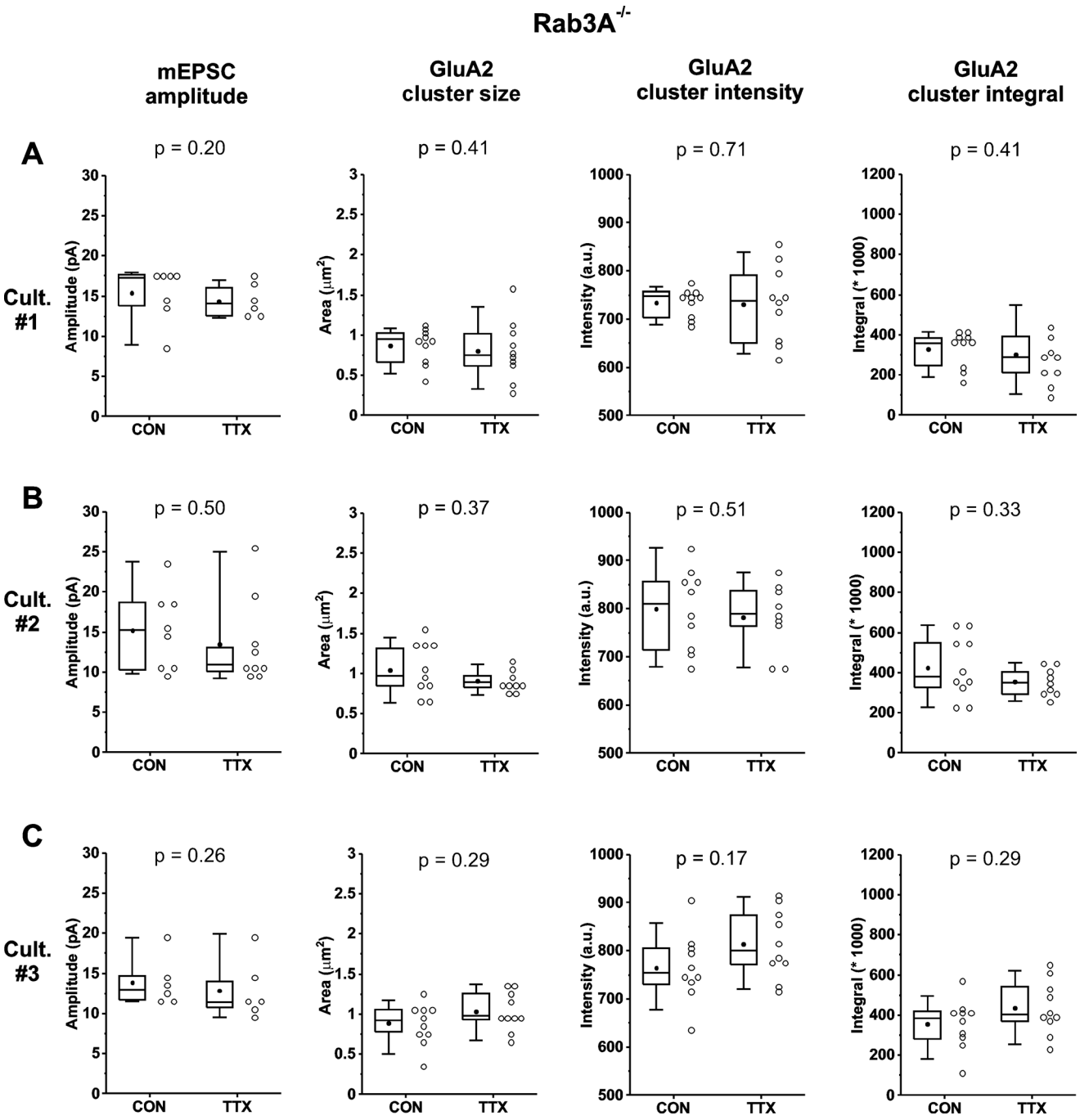

Figure 7. In cultures prepared from Rab3A$^{-/-}$ mice, a lack of effect of TTX treatment in mEPSC amplitudes was not always matched by a lack of effect in synaptic GluA2 receptor cluster characteristics.

(A) Culture #1: mean mEPSC amplitudes for pyramidal neurons from untreated coverslips (CON) and TTX-treated coverslips (TTX) (CON, N = 7, 15.4 ± 1.2 pA; TTX, N = 6, 14.4 ± 0.8 pA), compared to mean sizes, intensities, and integrals of synaptic GluA2 receptor clusters in images

taken of dendrites from other coverslips in the same culture (CON, N = 10, TTX, N = 10; size, CON, 0.87 ± 0.07 μm^2; TTX, 0.80 ± 0.12 μm^2; intensity, CON, 735 ± 10 A.U.; TTX, 731 ± 25 A.U.; integral, CON, 328,477 ± 28,250; TTX, 302,594 ± 53,052 A.U.). (B) Culture #2: mean mEPSC amplitudes for pyramidal neurons from untreated and TTX-treated coverslips (CON, N = 8, 15.2 ± 1.8 pA; TTX, N = 9, 13.5 ± 1.8 pA), compared to mean sizes, intensities, and integrals of synaptic GluA2 receptor clusters in images taken of dendrites from other coverslips in the same culture (CON, N = 10, TTX, N = 10; size, CON, 1.05 ± 0.10 μm^2; TTX, 0.93 ± 0.05 μm^2; intensity, CON, 800 ± 26 A.U.; TTX, 781 ± 21 A.U.; integral, CON, 425,552 ± 49,486 A.U.; TTX, 361,740 ± 21,963 A.U.). (C) Culture #3: mean mEPSC amplitudes for pyramidal neurons from untreated and TTX-treated coverslips (CON, N = 6, 13.9 ± 1.2 pA; TTX, N = 6, 12.9 ± 1.5 pA) compared to mean sizes, intensities, and integrals of synaptic GluA2 receptor clusters in images taken of dendrites from other coverslips in the same culture (CON, N = 10, TTX, N = 10; size, CON, 0.89 ± 0.08 μm^2; TTX, 1.03 ± 0.08 μm^2; intensity, CON, 765 ± 22 A.U.; TTX, 814 ± 23 A.U.; integral, CON, 354,279 ± 38,755 A.U.; TTX, 434,833 ± 42,350 A.U.). Cultures were fixed and processed for immunofluorescence on the same day as mEPSC recordings, and imaged within 1 week. Box plot parameters: box ends, 25th and 75th percentiles; whiskers, 10th and 90th percentiles; open circles represent means from individual cells; line, median; dot, mean. p values (shown on the graphs) are from Kruskal-Wallis test.

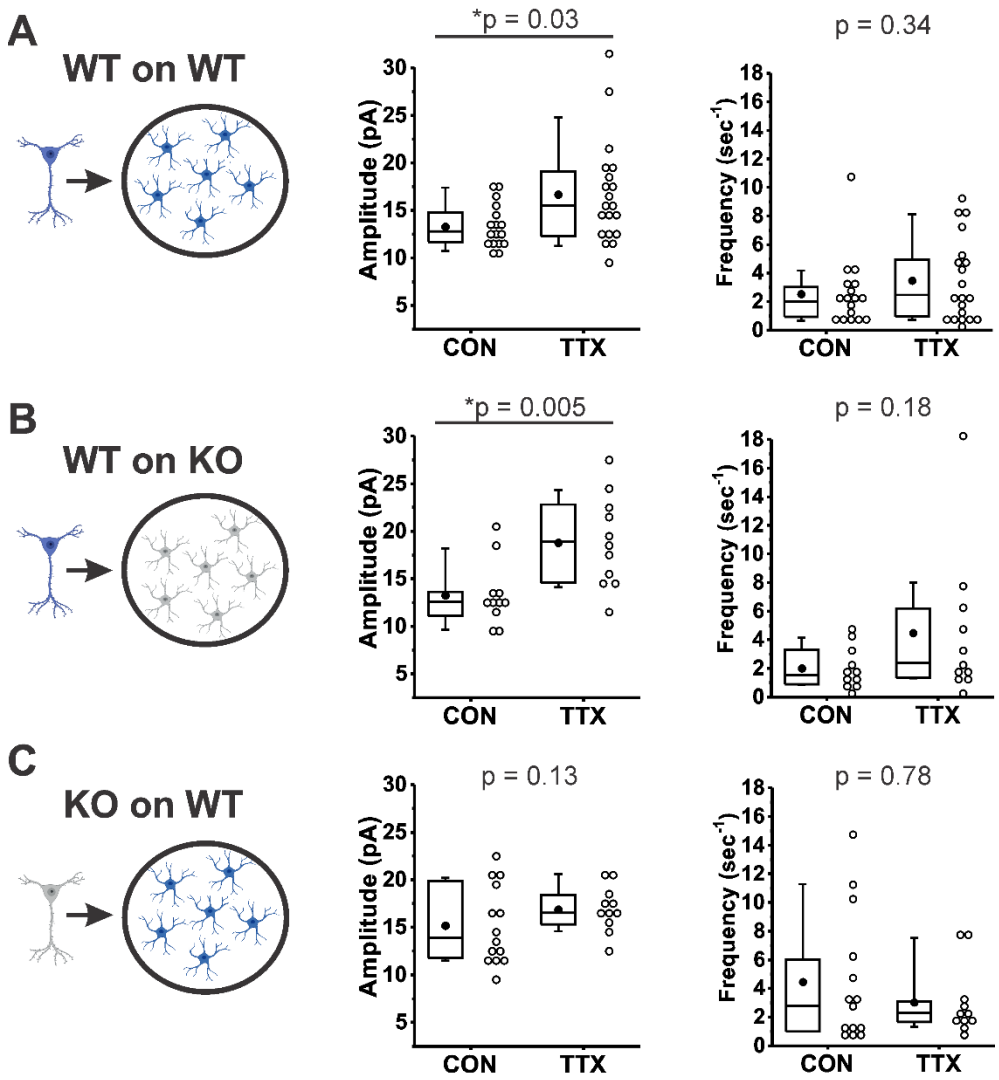

Figure 8. Rab3A in neurons, not astrocytes, was required for full TTX-induced homeostatic plasticity.

(A)-(C), mEPSC amplitude (Middle) and frequency (Right) data from dissociated cortical neurons plated on an astrocyte feeder layer, each prepared separately from the type of mice depicted in the schema (Left): (A) Neurons from Rab3A$^{+/+}$ mice plated on astrocytes from Rab3A$^{+/+}$ mice. Box plots for mEPSC amplitudes (CON, N = 17 cells, 13.3 ± 0.5 pA; TTX, N = 20 cells, 16.7 ± 1.2 pA) and mEPSC frequency in the same recordings (mean, CON, 2.54 ± 0.57 sec^{-1}; TTX, 3.48 ± 0.64 sec^{-1}); from 4 cultures. (B) Neurons from Rab3A$^{+/+}$ mice plated on astrocytes from Rab3A$^{-/-}$ mice. Box plots for average mEPSC amplitude (CON, N = 11 cells, 13.3 ± 1.0 pA; TTX, N = 11 cells, 18.8 ± 1.4 pA) and average mEPSC frequency in the same recordings (CON, 2.01 ± 0.41 sec^{-1}; TTX, 4.47 ± 1.53 sec^{-1}); from 2 cultures. (C) Neurons from Rab3A$^{-/-}$ neurons plated on astrocytes from Rab3A$^{+/+}$ mice. Box plots for average mEPSC amplitude (CON, N = 14 cells, 15.2 ± 1.1 pA;

TTX, N = 11 cells, 16.9 ± 0.7 pA) and mEPSC frequency in the same recordings (CON, 4.47 ± 1.21 sec^{-1}; TTX, 3.02 ± 0.70 sec^{-1}); from 3 cultures. Box plot parameters: box ends, 25th and 75th percentiles; whiskers, 10th and 90th percentiles; open circles represent means from individual cells; line, median; dot, mean. p values (shown on the graphs) are from Kruskal-Wallis test. p-values denoted with * and underline indicates significance of $p < 0.05$.

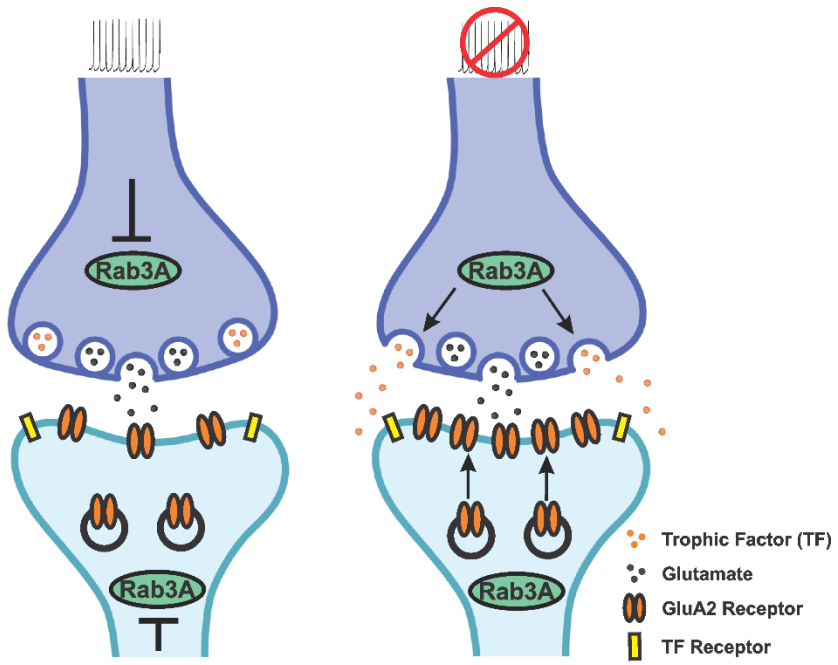

Figure 9. Model depicting the requirement for neuronal Rab3A in the homeostatic increase in synaptic GluA2 receptor levels after treatment with TTX.

Under normal activity levels (Left), neither presynaptic or postsynaptic Rab3A is engaged in the regulation of GluA2 receptor levels. After prolonged activity blockade (Right), Rab3A located in the presynaptic terminal promotes the release of a trophic factor (orange dots) that diffuses across the synapse and facilitates transport of postsynaptic vesicles containing GluA2 AMPA receptors (dark orange channels) to the surface membrane. Rab3A located in the postsynaptic dendrite directly promotes fusion of vesicles containing GluA2 AMPA receptors. Fusion of presynaptic vesicles containing glutamate (black dots) causes mEPSCs when glutamate binds to AMPA receptors. Adapted from “Synaptic Cleft” template, by BioRender.com (2024).

Table 1. Comparison of mEPSC amplitude and GluA2 receptor cluster characteristics in the same mouse cortical cultures prepared from Rab3A$^{+/+}$ mice, and another set of cultures prepared from Rab3A$^{-/-}$ mice. Data pooled from 3 cultures, and data from each of the 3 individual cultures.

	Rab3A$^{+/+}$ Pooled Data from 3 cultures				**Rab3A$^{-/-}$ Pooled Data from 3 cultures**			
Quantity	**CON Mean, SE (N)**	**TTX Mean, SE (N)**	**% change**	**p value**	**CON Mean, SE (N)**	**TTX Mean, SE (N)**	**% change**	**p value**
mEPSC amplitude	13.7 ± 0.9 pA (23)	16.4 ± 0.9 pA (24)	+19.7	*p = 0.02	14.9 ± 0.8 pA (21)	13.5 ± 0.9 pA (21)	-9.4	p = 0.18
GluA2 cluster size	0.90 ± 0.06 μm^2 (29)	1.08 ± 0.10 μm^2 (28)	+20.0	p = 0.27	0.93 ± 0.05 μm^2 (30)	0.91 ± 0.05 μm^2 (29)	-2.2	p = 0.75
GluA2 cluster intensity	684 ± 15 a.u. (29)	699 ± 12 a.u. (28)	+2.2	p = 0.15	766 ± 12 a.u. (30)	776 ± 15 a.u. (29)	+1.3	p = 0.46
GluA2 cluster integral	317898 ± 26726 a.u. (29)	389487 ± 41465 a.u. (28)	+22.5	p = 0.26	369436 ± 23439 a.u. (30)	364237 ± 25833 a.u. (29)	-0.8	p = 0.86
Quantity	**Rab3A$^{+/+}$ Culture #1**				**Rab3A$^{-/-}$ Culture #1 (not same culture as Rab3A$^{+/+}$)**			
mEPSC amplitude	14.2 ± 2.4 pA (6)	15.9 ± 1.9 pA (7)	+12.0	p = 0.25	15.4 ± 1.2 pA (7)	14.4 ± 0.8 pA (6)	-6.5	p = 0.20
GluA2 cluster size	0.73 ± 0.09 μm^2 (10)	0.89 ± 0.09 μm^2 (10)	+21.9	p = 0.45	0.87 ± 0.07 μm^2 (10)	0.80 ± 0.12 μm^2 (10)	-8.0	p = 0.41
GluA2 cluster intensity	682 ± 15 a.u. (10)	704 ± 11 a.u. (10)	+3.2	p = 0.13	735 ± 10 a.u. (10)	731 ± 25 a.u.	-0.5	p = 0.71
GluA2 cluster integral	256364 ± 35242 a.u. (10)	316647 ± 35077 a.u. (10)	+23.5	p = 0.29	328477 ± 28250 a.u. (10)	302594 ± 53052 a.u. (10)	-7.9	p = 0.41
Quantity	**Rab3A$^{+/+}$ Culture #2**				**Rab3A$^{-/-}$ Culture #2 (not the same culture as Rab3A$^{+/+}$)**			
mEPSC amplitude	13.8 ± 2.2 pA (7)	17.7 ± 1.8 pA (8)	+28.2	p = 0.16	15.2 ± 1.8 pA (8)	13.5 ± 1.8 pA (9)	-11.2	p = 0.50

GluA2 cluster size	0.91 ± 0.12 μm^2 (9)	1.42 ± 0.24 μm^2 (9)	+56.0	*p = 0.05	1.05 ± 0.10 μm^2 (10)	0.91 ± 0.04 μm^2 (9)	-13.3	p = 0.37
GluA2 cluster intensity	621 ± 14 a.u. (9)	679 ± 26 a.u. (9)	+9.3	*p = 0.04	800 ± 26 a.u. (10)	782 ± 23 a.u. (9)	-2.2	p = 0.51
GluA2 cluster integral	296300 ± 44108 a.u. (9)	512336 ± 96892 a.u. (9)	+72.9	*p = 0.04	425552 ± 49486 a.u. (10)	354289 ± 23099 a.u. (9)	-16.7	p = 0.33
Quantity	**Rab3A$^{+/+}$ Culture #3**				**Rab3A$^{-/-}$ Culture #3 (not the same culture as Rab3A$^{+/+}$)**			
mEPSC amplitude	13.4 ± 0.8 pA (10)	15.7 ± 1.0 pA (9)	+17.2	p = 0.10	13.9 ± 1.2 pA (6)	12.9 ± 1.5 pA (6)	-7.2	p = 0.26
GluA2 cluster size	1.05 ± 0.11 μm^2 (10)	0.95 ± 0.15 μm^2 (9)	-9.5	p = 0.46	0.89 ± 0.08 μm^2 (10)	1.03 ± 0.08 μm^2 (10)	+15.7	p = 0.29
GluA2 cluster intensity	744 ± 28 a.u. (10)	714 ± 25 A.U. (9)	-4.0	p = 0.29	765 ± 22 a.u. (10)	814 ± 23 a.u. (10)	+6.4	p = 0.17
GluA2 cluster integral	398870 ± 49500 a.u. (10)	347571 ± 65454 a.u. (9)	-12.9	p = 0.46	354279 ± 38755 a.u. (10)	434833 ± 42350 a.u. (10)	+22.7	p = 0.29

Table 2. Comparison of mEPSC amplitude and VGLUT1 positive presynaptic site characteristics in the same mouse cortical cultures prepared from Rab3A$^{+/+}$ and Rab3A$^{-/-}$ mice. Data pooled from 3 cultures, and data from individual cultures. mEPSC data are identical to that in Table 1, reproduced here for comparison purposes.

	Rab3A$^{+/+}$ Pooled Data from 3 cultures				**Rab3A$^{-/-}$ Pooled Data from 3 cultures**			
Quantity	**CON Mean, SE (N)**	**TTX Mean, SE (N)**	**% change**	**p value**	**CON Mean, SE (N)**	**TTX Mean, SE (N)**	**% change**	**p value**
mEPSC amplitude	13.7 ± 0.9 pA (23)	16.4 ± 0.9 pA (24)	+19.7	*p = 0.02	14.9 ± 0.8 pA (21)	13.5 ± 0.9 pA (21)	-9.4	p = 0.18
VGLUT1 site size	1.17 ± 0.08 μm^2 (29)	1.07 ± 0.06 μm^2 (24)	-7.7	p = 0.97	0.89 ± 0.03 μm^2 (30)	0.95 ± 0.04 μm^2 (29)	+6.7	p = 0.55
VGLUT1 site intensity	699 ± 39 a.u. (29)	639 ± 31 a.u. (28)	-8.6	p = 0.28	554 ± 13 a.u. (30)	570 ± 19 a.u. (29)	+2.9	p = 0.18
VGLUT1 site integral	430787 ± 36818 a.u. (29)	351653 ± 21689 a.u. (28)	-18.4	p = 0.13	257159 ± 18265 a.u. (30)	289857 ± 18521 a.u. (29)	+12.7	p = 0.21
Quantity	**Rab3A$^{+/+}$ Culture #1**				**Rab3A$^{-/-}$ Culture #1 (not same culture as Rab3A$^{+/+}$)**			
mEPSC amplitude	14.2 ± 2.4 pA (6)	15.9 ± 1.9 pA (7)	+12.0	p = 0.25	15.4 ± 1.2 pA (7)	14.4 ± 0.8 pA (6)	-6.5	p = 0.20
VGLUT1 site size	0.86 ± 0.06 μm^2 (10)	0.79 ± 0.04 μm^2 (10)	-8.1	p = 0.11	0.85 ± 0.04 μm^2 (10)	1.05 ± 0.07 μm^2 (10)	+23.5	p = 0.15
VGLUT1 site intensity	919 ± 35 a.u. (10)	832 ± 18 a.u. (10)	-9.5	p = 0.10	526 ± 17 a.u. (10)	629 ± 33 a.u. (10)	+19.6	p = 0.10
VGLUT1 site integral	445647 ± 39114 a.u. (10)	355055 ± 22354 a.u. (10)	-20.3	p = 0.07	233589 ± 16145 a.u. (10)	329851 ± 32856 a.u. (10)	+41.2	p = 0.10
Quantity	**Rab3A$^{+/+}$ Culture #2**				**Rab3A$^{-/-}$ Culture #2 (not same culture as Rab3A$^{+/+}$)**			
mEPSC amplitude	13.8 ± 2.2 pA (7)	17.7 ± 1.8 pA (8)	+28.2	p = 0.16	15.2 ± 1.8 pA (8)	13.5 ± 1.8 pA (9)	-11.2	p = 0.50

VGLUT1 site size	0.95 ± 0.09 μm^2 (9)	1.01 ± 0.05 μm^2 (9)	+6.3	p = 0.35	0.81 ± 0.05 μm^2 (10)	0.82 ± 0.03 μm^2 (9)	+1.2	p = 0.68
VGLUT1 site intensity	454 ± 19 a.u. (9)	459 ± 34 a.u. (9)	+1.1	p = 0.57	505 ± 14 a.u. (10)	538 ± 19 a.u. (9)	+6.1	p = 0.29
VGLUT1 site integral	239671 ± 29790 a.u. (9)	253222 ± 35117 a.u. (9)	+5.6	p = 0.96	213066 ± 19080 a.u. (10)	236927 ± 12964 a.u. (9)	+11.2	p = 0.41
Quantity	**Rab3A$^{+/+}$ Culture #3**				**Rab3A$^{-/-}$ Culture #3 (not same culture as Rab3A$^{+/+}$)**			
mEPSC amplitude	13.4 ± 0.8 pA (10)	15.7 ± 1.0 pA (9)	+17.2	p = 0.10	13.9 ± 1.2 pA (6)	12.9 ± 1.5 pA (6)	-7.2	p = 0.26
VGLUT1 site size	1.64 ± 0.13 μm^2 (10)	1.41 ± 0.10 μm^2 (10)	-13.4	p = 0.17	1.01 ± 0.05 μm^2 (10)	0.97 ± 0.07 μm^2 (10)	-4.0	p = 0.76
VGLUT1 site intensity	700 ± 33 a.u. (10)	608 ± 12 a.u. (10)	-13.1	*p = 0.02	568 ± 31 a.u. (10)	538 ± 35 a.u. (10)	-5.3	p = 0.55
VGLUT1 site integral	587932 ± 59742 a.u. (10)	436840 ± 31327 a.u. (10)	-25.7	*p = 0.05	324823 ± 42586 a.u. (10)	297499 ± 37637 a.u. (10)	-8.4	p = 0.82